Received: 8 September 2020 | Accepted: 15 March 2021

DOI: 10.1002/mma.7429

RESEARCH ARTICLE

WILEY

Micro-to-macro interactions in complex bodies: Wavelet-based post-processing detection

Anna Bosi[1] | **Paolo Maria Mariano**[2] | **Luca Salvatori**[2]

[1]Freelance Engineer, Nydalen allé 17,Oslo, N-0484, Norway

[2]DICEA, University of Florence, Florence, Italy

Correspondence
Paolo Maria Mariano, DICEA, Università di Firenze via Santa Marta 3, I-50139 Florence, Italy.
Email: paolomaria.mariano@unifi.it

Communicated by: W. Sprößig

We propose to couple finite element simulations and wavelet-based post-processing analysis to explore deeply the interaction degree of microscopic events on the gross behavior of complex bodies (which class includes metamaterials), above all around material or load discontinuities. After summarizing the theoretical structures our procedure refers to, as a sample case we select a special class of complex materials, namely, quasicrystals, and show how the proposed scheme works. As a result, we point out the effects of atomic rearrangements characterizing the quasicrystal structure on the stress field around a crack tip in static and dynamical setting. Our procedure can be also used for the analysis of dynamic experimental data. In this case, it allows us to detect discontinuities at least along directions selected within the body. In turn, our procedure can be used for monitoring purposes.

KEYWORDS

complex materials, cracks, finite elements, microstructures, quasicrystals, wavelets

MSC CLASSIFICATION

74A30; 74A35; 74A99; 74E99

1 | INTRODUCTION

We call *complex* those bodies in which microstructural events influence the gross behavior in a way hardly detectable by using only the traditional format of continuum mechanics (the one referred to Cauchy and later Truesdell's school axiomatization[1–3]). In that approach, in fact, a body is taken to be a set of so-called material elements, each identified with a point in the Euclidean space, so thought to be an indistinct piece of matter. Material complexity, in the sense sketched above, requires a more refined view on material elements: they behave as (and are in fact) systems, although at a microscopic scale. Their peculiar morphology, then, requires to be described through appropriate observable entities—call them *morphological descriptors* or *phase fields* (the latter a syntagma pertaining more specifically to Landau's theory of second-specie phase transitions). These descriptors can be vectors (as, e.g., in the case of quasicrystals, ferroelectrics, and magnetostrictive materials), elements of the projective plane (nematic liquid crystals), second-rank tensors (e.g., micromorphic and Casserat's materials), scalars (e.g., porous and multi-phase bodies), and so forth. In general, we may construct a model-building framework for the mechanics of complex materials by requiring that such descriptors belong to a differentiable manifold $\mathcal{M}$, taken commonly to have finite dimension,[4–6] which we often require to be complete and Riemannian when we explore existence of energy minimizers (i.e., equilibrium configurations) without embedding

$\mathcal{M}$ into a linear space,[7] otherwise the embedding is necessary[8]—it exists by Whitney's and Nash's theorems, but it is not unique.

Every descriptor $\nu \in \mathcal{M}$ transfers at macroscopic level information on the microscopic (*micro* to be defined for each specific) material texture. The general theoretical structure we may build up in this way requires to be specified when we look at specific material classes. Experimental evidences drive at least partially the process but, in turn, such a theoretical view addresses the design of metamaterials when they are constituted at least by two superposed and connected lattices (see,[9,10] although in the second reference the two-level lattice considered mimics a natural material[11–13]).

Computations help in visualizing and quantifying the mechanical behavior. Finite elements,[14,15] their extended version,[16] variational integrators,[17–19] and other methods may be profitably used, although even strong uncertainties in the result interpretation may appear, due to uncertain material parameter knowledge for the lack of appropriate experiments designed according to the multi-field approach we refer to here. In addition, we find at times problematic the exact assignment of boundary and initial conditions pertaining to the microstructure.

Then, such uncertainties render at times just of qualitative character the offspring of computations. Post-processing the resulting data may help at least in deepening their interpretation. For this reason, here we propose a mixing between finite elements and wavelet analyses. In particular, we propose to explore through wavelets micro-to-macro interactions at points where we have material or load discontinuities, such as tips (in the former case) or concentrated forces (in the latter). We follow a view introduced in Bosi[20] and Bosi et al.[21] to detect mechanical discontinuities through the analysis of wavelet spikes, a view investigated further in other studies[22–24] and references therein.

We show the procedure by referring in static and dynamic setting to a sample family of complex materials: quasicrystals. They are Aluminum-based alloys, with natural and synthetic origin, characterized by quasi-periodic arrangement of atoms, at variance of the basic requirements of classical crystallography.[25,26] Atomic rearrangements assure quasi-periodic structure by annihilating and reforming topological alterations of a periodic structure, the so-called *worms*. Such rearrangements exploit *inner* degrees of freedom. They are locally collected in a vector. Then, the manifold of microstructural shapes $\mathcal{M}$ coincides with $\mathbb{R}^3$, so in the sample case considered here, ν is a three-dimensional (3D) vector, reducing itself to two dimensions when we consider two-dimensional bodies.

We organize the present paper as follows: Section 2 collects basic elements on wavelets. Section 3describes the essential structure of the model-building framework for the mechanics of complex bodies. Section 4 introduces the special class considered here, namely, quasicrystals, in its physical and modeling peculiarities. Section 5 collects the finite element scheme and pertinent analyses in static and dynamic setting. Sections 6 includes wavelet post-processing of finite element results.

2 | BASIC NOTIONS ON WAVELETS

We recall here a few general remarks on wavelets; an extensive review can be found in the treatise.[27] For $\mathfrak{u}, s \in \mathbb{R}$ (with $\mathfrak{u}$ called a *translation* parameter and s a *scale* parameter), and $\psi \in L^2(\mathbb{R};\mathbb{C})$, we define a function family parameterized through $\mathfrak{u}$ and s, each element indicated by $\psi_{\mathfrak{u},s}$ and defined by

$$\psi_{\mathfrak{u},s}(t) := |s|^{-\frac{1}{2}} \psi\left(\frac{t-\mathfrak{u}}{s}\right).$$

We consider ψ such that

$$C_\psi := \int_{\mathbb{R}} \frac{|\hat{\psi}(\omega)|^2}{\omega} \, \mathrm{d}\omega < +\infty, \tag{1}$$

where $\hat{\psi}$ is the Fourier transform of ψ, while t and ω indicate, respectively, time and circular frequency. The bound (1), called an *admissibility condition*, implies that

(*i*) ψ is oscillatory with null average, i.e., $\hat{\psi}(0) = 0$ and $\int_{\mathbb{R}} \psi(t) \, \mathrm{d}t = 0$;
(*ii*) $|\hat{\psi}(\omega)|^2$ decays at least as ω^{-1} and $\psi(t) \to 0$ when $|t| \to \infty$.

We consider ψ as a *mother wavelet*. From it, we obtain so-called *daughter wavelets* by varying $\mathfrak{u}$ and s, tuning in this way frequency and time resolution.

For every $f \in L^2(\mathbb{R};\mathbb{C})$, we define the so-called *continuous wavelet transform* $W_\psi f$ by

$$(W_\psi f)(\mathfrak{u}, s) := \int_{\mathbb{R}} f(t)\bar{\psi}_{\mathfrak{u},s}(t)\ \mathrm{d}t,$$

where the overbar indicates complex conjugation. $W_\psi f$ is similar to a windowed Fourier transform in which the window length can change by varying s. Such a peculiar aspect makes wavelets well suited to analyze signals with sharp discontinuities and sudden changes.

With $j, k \in \mathbb{Z}$, by setting $s = s_0^j$ and $\mathfrak{u} = k\mathfrak{u}_0 s_0^j$, with s_0 fixed once and for all, we may define a discrete version of the wavelet transform by

$$(W_\psi f)(j,k) := \int_{\mathbb{R}} f(t)\bar{\psi}_{j,k}(t)\ \mathrm{d}t,$$

where

$$\psi_{j,k}(t) := s_0^{-\frac{j}{2}}\psi(s_0^{-j}t - k\mathfrak{u}_0 s_0^j).$$

Such a transform decomposes the function f in the discrete set of coefficients $(W_\psi f)(j, k)$. By restricting s to the dyadic scale 2^n, and assuming $\mathfrak{u}_0 = 1$, we reduce $\psi_{j,k}$ to

$$\psi_{j,n} := 2^{-\frac{j}{2}}\psi\left(\frac{t - 2^j n}{2^j}\right),$$

which is commonly used as essential tool for *multiresolution analysis* in which the main idea is to reconstruct f as a limit of successive approximations, each smoother than the preceding one, corresponding to a different level of resolution. The family $\{\psi_{j,n}\}_{(j,n)\in\mathbb{Z}^2}$ is an orthonormal basis in $L^2(\mathbb{R},\mathbb{R})$.

Several mother wavelets can be defined provided that the admissibility condition is satisfied. Their properties vary depending on symmetry (useful in avoiding de-phasing, above all in image processing), regularity (which is essential in signal reconstruction), and orthogonality (allowing fast algorithm and space-saving coding). Here, we select the *Haar wavelet*, which is largely used in crack detection, and the *biorthogonal* one; both show symmetry (see Mallat[27]). Haar's is the simplest family of wavelets with compact support. The functional basis is obtained by a multiresolution of piecewise constant functions. Biorthogonal wavelets have an explicit expression only in terms of piecewise splines. This latter family has symmetry, good numerical stability, and produces small wavelet coefficients in regular domains (for an extended treatment, see also Mallat[27]).

In previous definition, we have identified t as time. However, we can think of one-dimensional space domains, and the same definitions work. Wavelets on higher dimensional spatial domains can be also defined, but we do not explore their use here. Instead, we'll focus on time histories along appropriate (one-dimensional) sections in the body under analysis in the sample case considered.

3 | MULTI-FIELD VIEW ON THE MECHANICS OF COMPLEX BODIES: A SUMMARY

We have already defined above the way we speak of material complexity. In that sense, we have the need of describing the geometry of matter at low spatial scales, those pertaining to the microstructural events we refer to in each specific case considered. So, the construction of a framework for the mechanics of complex bodies starts from the representation of body morphology.

3.1 | Deformations and microstructural descriptors

We distinguish between *gross configuration* and *microstructural shapes*. The former is identified by a fit region $\mathcal{B}$ in the Euclidean space $\mathcal{E}$ (typical dimension may be 1, 2, or 3), which we take as reference and paragon setting to define the shapes we consider deformed with respect to it. Points in $\mathcal{B}$ are labeled by x. $\mathcal{B}$ is an arcwise connected domain with surface-like boundary, oriented by the normal n everywhere but a finite number of corners and edges. For the sake of generality, we define a non-singular metric g in $\mathcal{B}$ (i.e., the second-rank symmetric tensor g has non-null determinant at every point). g coincides with the identity tensor $\bar{I}$ when the frame (or frames) of reference considered is (or are) orthonormal.

We record gross shapes that we consider deformed with respect to $\mathcal{B}$ into a copy $\tilde{\mathcal{E}}$ (itself endowed with a non-singular metric $\tilde{g}$) of $\mathcal{E}$ through *deformations*, that is, orientation preserving differentiable maps $x \mapsto y := \tilde{y}(x) \in \tilde{\mathcal{E}}$, with derivative $D\tilde{y}(x)$ indicated by F. Take a basis $\{\mathbf{e}_A\}$ in a neighborhood of $x \in \mathcal{B}$, with dual counterpart $\{\mathbf{e}^A\}$, defined by $\mathbf{e}^A \cdot \mathbf{e}_B = \delta^A_B$, with δ^A_B the Kronecker delta, A and B running from 1 to the dimension of $\mathcal{E}$; the dot indicates from now on duality pairing. Take another basis $\{\tilde{\mathbf{e}}_i\}$ in a neighborhood of $y := \tilde{y}(x)$, with dual counterpart $\{\tilde{\mathbf{e}}_i\}$. With respect to these bases, g reads as $g = g_{AB}\mathbf{e}^A \otimes \mathbf{e}^B$ while $\tilde{g} = \tilde{g}_{ij}\tilde{\mathbf{e}}^i \otimes \tilde{\mathbf{e}}^j$, and the linear operator F has the form $F = F^i_{\ A}\tilde{\mathbf{e}}_i \otimes \mathbf{e}^A$, where $\otimes$ indicates tensor product and we assume summation over repeated indices. We adopt for F the standard nomenclature and call it as a *deformation gradient*, although the gradient of $\tilde{y}$, namely, $\nabla\tilde{y}(x)$ in the same bases reads $\nabla\tilde{y}(x) = (\nabla\tilde{y}(x))^{iA}\tilde{\mathbf{e}}_i \otimes \mathbf{e}_A$. The metric g establishes a link between the two; in fact, $F = \nabla\tilde{y}(x)g$, or, more explicitly, $F^i_{\ A} = (\nabla\tilde{y}(x))^{iB}g_{BA}$. When the frames of reference are orthonormal, that is, metrics coincide with the second-rank identity tensor, we may identify F with $\nabla\tilde{y}(x)$; otherwise, the role of the metric needs to be considered. This happens also when we define two linear operators associated with F, namely, its transpose F^T and its formal adjoint F^*. In terms of components, the former reads $F^\mathsf{T} = F^A_{\ i}\mathbf{e}_A \otimes \tilde{\mathbf{e}}^i$, while the latter $F^* = F_A^{\ i}\mathbf{e}^A \otimes \tilde{\mathbf{e}}_i$. The metric links F^T and F^*: in fact, we have $F^\mathsf{T} = g^{-1}F^*\tilde{g}$, that is, in components $F^A_{\ i} = g^{AB}F_B^{\ j}\tilde{g}_{ji}$, where g^{AB} is the standard notation for the ABth component of the inverse metric g^{-1}. When both g and $\tilde{g}$ coincide with the second-rank identity tensor, F^T and F^* may be identified with each other. In the present setting, the *deformation tensor* E for finite strain is defined by $E = \frac{1}{2}(C-g)$, where C is the so-called *right Cauchy–Green* tensor and is given by $C = F^*\tilde{g}F$, that is, in components $C = C_{AB}\mathbf{e}^A \otimes \mathbf{e}^B = F_A^{\ i}\tilde{g}_{ij}F^j_{\ B}\mathbf{e}^A \otimes \mathbf{e}^B$, namely, C is the pull-back in reference place, through deformation $\tilde{y}$, of the spatial metric $\tilde{g}$, so that E takes the role of a difference between the two metrics. More common is a version of E given by $\tilde{E} := g^{-1}E = \frac{1}{2}(g^{-1}C-I) = \frac{1}{2}(g^{-1}F^*\tilde{g}F-g^{-1}g) = \frac{1}{2}(F^\mathsf{T}F-\bar{I})$, with $\bar{I} = \delta^A_{\ B}\mathbf{e}_A \otimes \mathbf{e}^B$. With $\imath : \mathcal{E} \to \tilde{\mathcal{E}}$ the identification map between $\mathcal{E}$ and its copy $\tilde{\mathcal{E}}$, we commonly define a *displacement* as the vector field $\tilde{u}$ with values $u := \tilde{u}(x) = \tilde{y}(x)-\imath(x)$. Consequently, $F = Du + I$, with $I = \delta^i_{\ A}\tilde{\mathbf{e}}_i \otimes \mathbf{e}^A$ the shifter between $\mathcal{E}$ and $\tilde{\mathcal{E}}$, so that $I^\mathsf{T}I = \bar{I}$, and $\tilde{E}$ becomes $\tilde{E} = \mathrm{sym}(D\bar{u}) + \frac{1}{2}(Du)^\mathsf{T}Du$, where $\bar{u} := I^\mathsf{T}u = \delta^A_{\ i}u^i$ and sym extracts the symmetric part of its argument. The condition $|Du| << 1$ defines, as usual, the small-strain regime, which we will refer to in the specific analyses reported below. In such a regime, we do not distinguish between the reference gross shape $\mathcal{B}$ and its deformed counterpart $\mathcal{B}_c = \tilde{y}(\mathcal{B})$, so that we'll not distinguish between uppercase and lowercase indices, opting for the latter writing.

We describe microstructural shapes coarsely by assigning a differentiable map $x \mapsto \nu := \tilde{\nu}(x) \in \mathcal{M}$, with x ranging in $\mathcal{B}$. At each x, the (observable) variable ν summarizes the essential features of the microstructural shape we are interested in, those we consider to be essential. Its choice is a matter of modeling when we tackle the analysis of a specific class of complex bodies. In general, we say that ν belongs to a finite-dimensional differentiable manifold $\mathcal{M}$, and we call it *manifold of microstructural shapes*. Such a choice does not depend on a sense for abstraction, which could appear useless for applications at a first glance. Rather it is a matter of simplicity. In other words, we clearly say that to construct a general model-building framework for the mechanics of complex materials we need just that the set $\mathcal{M}$ where we select morphological descriptors be a differentiable manifold—this property is the minimal need. Such a choice allows us to construct a unified theory. Precisely, $\mathcal{M}$ is a set endowed with a topology allowing us to distinguish between two of its elements whatever their choice be, which is locally Euclidean. This means that we may select possibly intersecting subsets able to cover $\mathcal{M}$ and we can assign coordinate charts in each of them in a way that we can change frames going from one subset to another. Locally, the dimensions of coordinate charts define a dimension of the manifold. When differentiable functions of class C^k describe the change of frames, we affirm that the manifold is differentiable of class C^k; when $k = +\infty$ we do not specify the class. Over $\mathcal{M}$, we find naturally the notion of tangent at ν, as an equivalent class of smooth curves agreeing in a neighborhood of ν, and indicate the pertinent tangent space collecting all the possible tangent elements at ν, indicating it by $T_\nu\mathcal{M}$. We write $T^*_\nu\mathcal{M}$ for its dual, that is, the space of all linear maps over $T_\nu\mathcal{M}$. It is not a linear space, but the union $T\mathcal{M} := \bigcup_{\nu\in\mathcal{M}} T_\nu\mathcal{M}$, called a *tangent bundle*, is not a linear space, unless $\mathcal{M}$ itself is a linear space. As a matter of fact, $\mathcal{B}$ is itself a differentiable manifold, one embedded in the Euclidean space $\mathcal{E}$. A basic difference with the manifold of microstructural shapes is that we consider $\mathcal{M}$ in general not embedded in any linear space, although it could be, being finite-dimensional. We indicate by N the derivative $D\tilde{\nu}(x)$. With $\hat{\mathbf{e}}_\alpha$ the αth element of the basis in a coordinate chart pertaining to a neighborhood of $\nu = \tilde{\nu}(x)$, the linear operator N takes the form $N = N^\alpha_{\ A}\hat{\mathbf{e}}_\alpha \otimes \mathbf{e}^A = \frac{\partial\nu^\alpha}{\partial x^A}\hat{\mathbf{e}}_\alpha \otimes \mathbf{e}^A$. The map $\tilde{\nu}$ describes microstructural morphology in Lagrangian representation because it is defined over the reference shape. We could choose a Eulerian representation by defining a map $\tilde{\nu}_c := \tilde{\nu}\circ\tilde{y}^{-1}$. We do not explore further this option because in the linear setting we refer to for the explicit analyses collected below, we do not distinguish between Lagrangian and Eulerian representation. Itself ν could contribute to the definition of strain measures, depending on its physical meaning selected in specific circumstances. The Cosserat scheme is a paradigmatic example: in that case, ν describes a local rigid rotation—every material element is intended as a small rigid body able to rotate independently of its neighbors—which

affects strain measures, as it occurs in direct models of rods (see Ericksen and Truesdell[28]). In general, we can just say that for complex bodies, gross strain measures are symmetric-tensor-valued maps depending on $\tilde{y}$, $\tilde{g}$, g, $\tilde{v}$, F, N, or even $g_{\mathcal{M}}$, the metric on $\mathcal{M}$, when we consider it to be Riemannian, which vanish when $F = I$ (see for additional details Mariano[6,29]). Less uncertain is the definition of *motions*, which have to be considered here, in extended sense, as pairs of time-parameterized differentiable maps: $(x, t) \mapsto (y, \nu) := (\tilde{y}(x, t), \tilde{\nu}(x, t)) \in \tilde{\mathcal{E}} \times \mathcal{M}$, with the possibility of substituting $\tilde{y}$ with the displacement map $\tilde{u}$. Pertinent velocities are then $\dot{y} := \frac{\mathrm{d}\tilde{y}(x,t)}{\mathrm{d}t}$ and $\dot{\nu} := \frac{\mathrm{d}\tilde{\nu}(x,t)}{\mathrm{d}t}$ in Lagrangian representation, that is, as fields defined over $\mathcal{B}$. We may consider the Eulerian velocity field $v := \tilde{v}(y, t)$, and we know that $\dot{y} = v$ at every point and instant. The same property does not hold for $\dot{\nu}$. In Eulerian representation, the microstructure descriptor time rate is, in fact, $\upsilon := \frac{\mathrm{d}\tilde{\nu}_c(y,t)}{\mathrm{d}t} = \frac{\partial\tilde{\nu}_c(y,t)}{\partial t} + D_y\tilde{\nu}_c(y, t)\dot{y} = \frac{\partial\tilde{\nu}_c(y,t)}{\partial t} + D_y\tilde{\nu}_c(y, t)v$.

3.2 | Rules for changes in observers

The present setting requires a view on observers a bit more extended than usual because with consider ν as an observable entity. According to a proposal in Mariano,[30] we define an *observer* to be the set of *frames of reference (frames in short) assigned on all spaces necessary to describe the shape of a body and its motion*. So, an observer is composed by an atlas of coordinates over the physical $\tilde{\mathcal{E}}$, another over the reference space $\mathcal{E}$, one over the manifold of microstructural shapes $\mathcal{M}$, a time scale. Once we accept such a definition, a key point is the choice of changes in observers. For the purposes of this summary, we just select changes in observers that leave invariant the time scale, the reference space, and alter coordinate frames in $\tilde{\mathcal{E}}$ by a rigid-body motion. Write $\mathcal{O}$ and $\mathcal{O}'$ for two different observers. A place y for $\mathcal{O}$ becomes y' for $\mathcal{O}'$, with $y' := \mathfrak{a}(t) + Q(t)\,(y - y_0)$, where $\mathfrak{a}(t)$ and $Q(t)$ are the values at t of time-differentiable maps $t \mapsto \mathfrak{a}(t) \in \mathbb{R}^3$, $t \mapsto Q(t) \in SO(3)$, with t running in the selected time interval, and y_0 an arbitrary point in space. The velocities in Lagrangian representation are then $\dot{y}$ for the first observer and $\dot{y}' = \dot{\mathfrak{a}} + \dot{Q}\,(y - y_0) + \dot{y}$ for the second. By rotating back through the action of $Q^{-1} = Q^T$ the rate $\dot{y}'$ into the frame defining $\mathcal{O}$, and indicating by $\dot{y}^\diamond$ the rotated velocity, that is, $\dot{y}^\diamond := Q^T\dot{y}'$, we get

$$\dot{y}^\diamond := \mathfrak{c} + q \times (y - y_0) + \dot{y},$$

where $\mathfrak{c} := Q^T\dot{\mathfrak{a}}$ is a translational rigid velocity, q the axial vector of the skew-symmetric tensor $Q^T\dot{Q}$, both depending on time only, and $\times$ indicates the vector product. In terms of displacement, we have $\dot{u}^\diamond = \mathfrak{c}(t) + q(t) \times (y - y_0) + \dot{u}$. Since $\dot{y}(x, t) = \dot{u}(x, t) = v(y, t)$, we can also write $\mathrm{v}^\diamond := \mathfrak{c}(t) + q(t) \times (y - y_0) + \mathrm{v}$.

The choice of representing the body morphology in two distinct spaces—gross configuration selected $\tilde{\mathcal{E}}$ and microstructural shapes described through the introduction of $\mathcal{M}$—is just matter of modeling. Microstructures are, in fact, in the physical space. When we translate frames of reference in that space, the representation of microstructures does not change. Microstructural changes are *relative* to the material element they occur within. In this sense, they are *inner* degrees of freedom, but not internal variables in the sense of non-equilibrium thermodynamics, that is, non-observable entities measuring the detachment from thermodynamic equilibrium through dissipation. They contribute to the (conservative) equilibrium, so they are observable. And although translation does not change their description, the frame of reference rotations may alter microstructure representation. However, not always the action of $SO(3)$ over the manifold $\mathcal{M}$ is defined. For this reason, we introduce a *link* between observer changes in $\mathcal{E}$ and the group of diffeomorphisms (i.e., one-to-one differentiable maps with differentiable inverse) of $\mathcal{M}$ onto itself, namely, $\mathrm{Diff}(\mathcal{M}, \mathcal{M})$, through a family of differentiable homomorphisms $\{\lambda\}$, each being a map $\lambda : SO(3) \to \mathrm{Diff}(\mathcal{M}, \mathcal{M})$, a family which can be even empty. At the moment, we do not need to specify the nature of λ. We just need to render explicit the rule linking $\dot{\nu}$, as measured by a given observer, to the value $\dot{\nu}^\diamond$, which is the pull-back to first observer of ν time rate measured by another one. It reads

$$\dot{\nu}^\diamond = \dot{\nu} + \mathcal{A}(\nu)q.$$

$\mathcal{A}(\nu)$ is at each $\nu \in \mathcal{M}$ a linear operator mapping vectors of $\mathbb{R}^3$ onto elements of the tangent space $T_\nu\mathcal{M}$ of $\mathcal{M}$ at ν. When $SO(3)$ does not act on$\mathcal{M}$ and the set $\{\lambda\}$ is not empty, with $\nu_{\lambda(Q)}$, the value of ν after the action of $\lambda\,(Q) \in \mathrm{Diff}(\mathcal{M}, \mathcal{M})$, the linear operator $\mathcal{A}(\nu)$ is given by $\mathcal{A}(\nu) = \frac{d\nu_{\lambda(Q)}}{d\lambda}\frac{d\lambda(Q)}{d\mathrm{q}}\Big|_{\mathrm{q}=0}$, where $\mathrm{q}(\tau) \in \mathbb{R}^3$ is at instant τ the rotational speed of observer change in the physical space.Finally, when $SO(3)$ is a subgroup of $\mathrm{Diff}(\mathcal{M}, \mathcal{M})$ (typical examples occur when $\mathcal{M}$ coincides with $\mathbb{R}^3$, the unit ball in $\mathbb{R}^3$, or a tensor space modeled over $\mathbb{R}^3$), we write $\mathcal{A}(\nu) = \frac{d\nu_{\mathrm{q}}}{d\mathrm{q}}\Big|_{\mathrm{q}=0}$.

3.3 | Macro and micro interactions

In the traditional format of continuum mechanics, we presume that interactions among material elements of a body and with the external environment are classified into contact and bulk ones, say $\mathfrak{t}$ and $b^{\ddagger}$, respectively, the latter being sum of inertial (indicated by a superscript *in*) and non-inertial components, namely, $b^{\ddagger} = b + b^{in}$, say in Lagrangian representation. According to Capriz,[4] we *assume* the same classification for interactions at microstructural level, so we write τ for microstructural contact interactions and $\beta^{\ddagger}$ for the bulk ones, presuming even in this case additive decomposition into inertial and non-inertial components, namely, $\beta^{\ddagger} = \beta + \beta^{in}$. By following the proposals in Mariano[5] (further refined in Mariano[6]), we define such interactions on a generic part $\mathfrak{b}$ of $\mathcal{B}$, so in the reference configuration, through the *external power* $\mathcal{P}^{ext}_{\mathfrak{b}}$ performed on $\mathfrak{b}$ in all mechanisms altering gross and microstructural body shapes. Then, we write $\mathcal{P}^{ext}_{\mathfrak{b}}$ as

$$\mathcal{P}^{ext}_{\mathfrak{b}}(\dot{y},\dot{\nu}) := \int_{\mathfrak{b}} \left(b^{\ddagger}\cdot\dot{y} + \beta^{\ddagger}\cdot\dot{\nu}\right) \mathrm{d}\mu(x) + \int_{\partial\mathfrak{b}} (\mathfrak{t}_{\partial}\cdot\dot{y} + \tau_{\partial}\cdot\dot{\nu})\,\mathrm{d}\mathcal{H}^2(x),$$

where $d\mu(x)$ is the standard volume measure and $\mathrm{d}\mathcal{H}^2(x)$ the surface one. Subscript ∂ associated with the contact actions indicates that *we presume dependence* of $\mathfrak{t}$ and τ *on the boundary* $\partial\mathfrak{b}$. We subordinate $\mathcal{P}^{ext}_{\mathfrak{b}}$ to *invariance* under isometry-based changes in observers as defined above, taking it as a basic axiom. Precisely, we ask that $\mathcal{P}^{ext}_{\mathfrak{b}}(\dot{y},\dot{\nu}) = \mathcal{P}^{ext}_{\mathfrak{b}}\left(\dot{y}^{\circ},\dot{\nu}^{\circ}\right)$ *for any choice of* $\mathfrak{b}$, $\mathfrak{c}$, and q. The axiom implies a more specific representation of interactions at macroscopic and microscopic scale, and their balance. In the proposition below, we avoid to write explicitly time for the sake of conciseness, but the fields considered have to be intended as time dependent when motions enter into play.

Proposition 1.

(1) The integral balances

$$\int_{\mathfrak{b}} b^{\ddagger}\ \mathrm{d}\mu(x) + \int_{\partial\mathfrak{b}} \mathfrak{t}_{\partial}\ \mathrm{d}\mathcal{H}^2(x) = 0,$$

$$\int_{\mathfrak{b}} \left((y-y_0)\times b^{\ddagger} + \mathcal{A}^{*}\beta^{\ddagger}\right)\mathrm{d}\mu(x) + \int_{\partial\mathfrak{b}} ((y-y_0)\times\mathfrak{t}_{\partial} + \mathcal{A}^{*}\tau_{\partial})\,\mathrm{d}\mathcal{H}^2(x) = 0$$

hold. $\mathcal{A}^{*}$ is the formal adjoint of $\mathcal{A}$, that is, $\mathcal{A}^{*}(\nu)$ is a linear operator from $T^{*}_{\nu}\mathcal{M}$ to $\mathbb{R}^3$.

(2) If $\left|b^{\ddagger}\right|$ is bounded over $\mathcal{B}$, and $\mathfrak{t}$ is a continuous function of x, the standard traction $\mathfrak{t}$ satisfies the action-reaction principle and depends on $\partial\mathfrak{b}$ only through the normal n to it in all points where it is well-defined. Then, we can write $\mathfrak{t}_{\partial} = \mathfrak{t} := \tilde{\mathfrak{t}}(x,n) = -\tilde{\mathfrak{t}}(x,-n)$. Also, as a function of n, $\tilde{\mathfrak{t}}$ is homogeneous and additive, that is, there exists a second-rank tensor field $x \mapsto P(x)$ such that $\tilde{\mathfrak{t}}(x,n) = P(x)n(x)$, where

$$P(x) = \sum_{K=1}^{3} \tilde{\mathfrak{t}}(x,e_K)\otimes e_K \in \mathrm{Hom}(T^{*}_{x}\mathcal{B}, T^{*}_{u(x)}u(\mathcal{B}))$$

is the so-called first Piola–Kirchhoff stress.

(3) If in addition $\left|\mathcal{A}^{*}\beta^{\ddagger}\right|$ is bounded over $\mathcal{B}$ and τ_{∂} is a continuous function of x, the microstructural contact action τ_{∂} satisfies a non-standard action-reaction principle and depends on $\partial\mathfrak{b}$ only through the normal n to it in all points where it is well-defined, namely, $\mathcal{A}^{*}(\tilde{\tau}(x,n) + \tilde{\tau}(x,-n)) = 0$. Also, as a function of n, $\tilde{\tau}$ is homogeneous and additive, that is, there exists a second-rank tensor field $x \mapsto \mathcal{S}(x)$ such that $\tilde{\tau}(x,n) = \mathcal{S}(x)n(x)$. We call

$$\mathcal{S}(x) = \sum_{K=1}^{3} \tilde{\tau}(x,e_K)\otimes e_K \in \mathrm{Hom}(T^{*}_{x}\mathcal{B}, T^{*}_{\nu}\mathcal{M})$$

a microstress in Lagrangian representation.

(4) If the fields $x \mapsto P$ and $x \mapsto \mathcal{S}$ are in $C^1(\mathcal{B}) \cap C\left(\bar{\mathcal{B}}\right)$ and the fields $x \mapsto b$, $x \mapsto \beta^{\ddagger}$ are continuous over $\mathcal{B}$, the pointwise balance of forces

$$Div\ P + b^{\ddagger} = 0 \tag{3}$$

holds, and there exists a field $x \mapsto z(x) \in T^{*}_{\nu}\mathcal{M}$ such that

$$Div\ \mathcal{S} + \beta^{\ddagger} - z = 0 \tag{4}$$

and

$$skw\ PF^* = \frac{1}{2}\mathsf{e}\left(\mathcal{A}^* z + (D\mathcal{A}^*)\, S\right). \tag{5}$$

(5) The identity

$$\mathcal{P}^{ext}_{\mathfrak{b}}(\dot{y}, \dot{\nu}) = \int_{\mathfrak{b}} \left(P \cdot \dot{F} + z \cdot \dot{\nu} + S \cdot \dot{N}\right) \mathrm{d}\mu(x) \tag{6}$$

holds, and we call internal(or inner) power the right-hand side term.

The previous proposition is a refinement of results in other studies.[5,6,29] It can be proven also in less stringent conditions. Precisely, we could only require that the bulk terms in the integral balances at item (1) be Radon measures and that the contact interactions be bounded. In this case, pointwise balances would hold just in weak sense, which is eventually what we require in constructing finite elements.

The inner bulk action z is a *microstructural self-action*. It is strictly due to the insensitivity of ν to rigid translations of material elements into the physical space $\tilde{\mathcal{E}}$. In the traditional format of continuum mechanics, a self-action does not appear at macroscopic scale because ν is sensitive to translations of reference frames, as dictated by the rule determining $\nu^\diamond$. The existence of z at microstructural level is a peculiarity of the mechanics of complex bodies. Besides formal aspects just recalled, it emerges because the description of microstructures within a material element is *relative* to the gross behavior of the material element itself.

3.4 | A priori restrictions on constitutive structures: Considering the elastic case and a special form of dissipation

Consider here isothermal setting. The standard use of a mechanical dissipation inequality furnishes a priori restrictions on constitutive structures. The only variation with respect to the version adopted in the traditional format of continuum mechanics is the presence of right-hand side term in equation (6). With ψ the *free energy density (and some abuse of notation with respect to Section 2)*, for the mechanical dissipation inequality we write

$$\frac{\mathrm{d}}{\mathrm{d}t}\int_{\mathfrak{b}} \psi \ \ \mathrm{d}\mu(x) - \int_{\mathfrak{b}} \left(P \cdot \dot{F} + z \cdot \dot{\nu} + S \cdot \dot{N}\right) \mathrm{d}\mu(x) \leq 0$$

for any choice of the rate fields involved. Equality holds in the conservative case in which ψ reduces to the *elastic energy density e*. Assume, for example, that $\psi = \tilde{\psi}(F, \nu, N)$, $P = \tilde{P}(F, \nu, N)$, $z = \tilde{z}(F, \nu, N)$, and $S = \tilde{S}(F, \nu, N)$. By computing the time derivative of ψ (the part $\mathfrak{b}$) is in $\mathcal{B}$, which is here fixed once and for all), and exploiting the arbitrariness of $\dot{F}$, $\dot{\nu}$, and $\dot{N}$, we get

$$P = \frac{\partial \psi}{\partial F}, \quad z = \frac{\partial \psi}{\partial \nu}, \quad S = \frac{\partial \psi}{\partial N}.$$

Their counterparts in the current configuration $\mathcal{B}_c$ are given by

$$\sigma = \frac{1}{\det F}\frac{\partial \psi}{\partial F}F^*, \quad z_c = \frac{1}{\det F}\frac{\partial \psi}{\partial \nu}, \quad S_c = \frac{1}{\det F}\frac{\partial \psi}{\partial N}F^*,$$

where σ is the standard *Cauchy stress*.

Dissipation can be accounted for in various ways. Here we just make an example pertinent to the special case considered below. We consider dissipation at microstructural level just inside each material element. We maintain the same constitutive choices above with the exception of $z = \tilde{z}(F, \nu, N)$, replaced now by the assumption that z is the sum of energetic-type (z^e) and dissipative (z^d) components, namely, $z = \tilde{z}^e(F, \nu, N) + \tilde{z}^d(F, \nu, N, \dot{\nu})$. The procedure above implies the same results with the exception of z, which is given by

$$z = \frac{\partial \psi}{\partial \nu} + \tilde{z}^d(F, \nu, N, \dot{\nu}),$$

with z^d satisfying the inequality $z^d \cdot \dot{\nu} \geq 0$, for any choice of $\dot{\nu}$; it implies

$$z^d = a(\ldots)\dot{\nu}$$

with $a(\ldots)$ a real-positive-valued state function, often chosen to be a scalar.

4 | THE SPECIAL CLASS OF COMPLEX MATERIALS CONSIDERED IN SIMULATIONS DEVELOPED HERE: QUASICRYSTALS

4.1 | Physical structure

In 1991, the International Union of Crystallography changed the definition of crystal, considered currently just as "any solid having an essentially discrete diffraction diagram."[31] This definition cancels the traditional requirement of periodicity for the distribution of Bragg's peaks in the diffraction diagram. Then, it accepts quasi-periodic structures, those discovered by D. Shechtman in 1982, who realized that rapid cooled Aluminium-based alloys diffract electrons in a way such that they generate Bragg's peak patterns incompatible with lattice translations, a discovery disseminated 2 years later in Shechtman et al.[25] This result influenced the definition of crystal after it was clear that such quasi-periodicity was not due to complicated twin structures, those presumed by L. Pauling in a strong criticism to Shechtman's results. Presently, we know the existence of *natural* quasi-periodic crystals, called *quasicrystals*, discovered in meteorites.[32] Long-range incompatible order with periodic tessellation of 3D ambient space characterizes their structure, for example, icosahedral phases in 3D space or pentagonal ones in the plane.

When we consider a 3D quasi-periodic lattice and we expand in Fourier series the mass density, we find a six-dimensional wave vector strictly induced by the quasi-periodic nature of the underlying lattice. It can be viewed, in fact, as the orthogonal projection of a higher dimensional periodic lattice onto an incommensurate subspace of the space including it (see, e.g., Dubois[26]). Specifically, a one-dimensional quasi-periodic lattice emerges by taking a two-dimensional periodic atomic array with square symmetry, a straight line inclined by an irrational angle with respect to the main axes of the square symmetry, and projecting atoms over the line in orthogonal direction. More in general, a quasi-periodic lattice in $n-$dimensional space can be viewed as a projection of a periodic lattice in space with double dimension over an incommensurate subspace of it. The circumstance suggested to construct quasicrystal mechanics as a standard continuum mechanics in a higher dimensional space (see, e.g., other studies[33–35]). Projection on the incommensurate subspace gives rise to the common displacement field, with related standard bulk and contact actions, while what remains in the orthogonal space is depicted by a vector field containing degrees of freedom called *phasons*, with associated bulk and contact actions. A question is whether such a view on quasicrystal continuum mechanics is complete or requires a deeper analysis. The question stands on what we really do when we construct a continuum description of quasicrystals (i.e., we analyze them in long wavelength approximation), or better, and more precisely, what we think that phason degrees of freedom are. Currently, we consider phasons as *atomic flips*, that is, localized atom rearrangements that assure quasi-periodicity in space (see other studies[36–38]) through the construction of atomic clusters with symmetry different from the prevailing one—the so-called *worms* (see, e.g., Penrose's tiling to have a figurative appearance of such structures). This view suggests us that the phason vector attached at a point can be, in fact, interpreted as an entity collecting the degrees of freedom exploited by atomic flips *within* the patch of matter (a material element in continuum mechanics jargon) the properties of which are associated with that point. The interpretation has non-trivial consequences. As relative changes within every material element (i.e., every characteristic structural entity defining the quasi-periodic lattice—an icosahedron, a pentagon, etc.), phasons are insensitive to rigid translations of frames in the physical space, and this implies the existence of a phason self-action, as proven in Mariano and Planas.[39] Then, the representation of quasicrystal mechanics falls naturally in the general model-building framework for the mechanics of complex bodies as summarized in the previous section. Special choices are necessary in the general model-building framework. In the limit case of vanishing phason self-action, the analysis in elastic setting reduces to consider standard elasticity in a space with dimension higher than the ambient one (see other studies among several references in this reduced setting[40–44]).

4.2 | Mechanics of quasicrystals, a special class of complex bodies

4.2.1 | General modeling choices for quasicrystals

We choose the manifold of microstructural shapes $\mathcal{M}$ to be coincident with $\mathbb{R}^3$. Then, ν is for quasicrystals a vector. The differentiable map $(x,t) \mapsto \nu := \tilde{\nu}(x,t) \in \mathbb{R}^n$ is the so-called *phason field*.

In this case, $\mathcal{A}(\nu) = -q\times$, with $q \in \mathbb{R}^3$ the rotation velocity vector pertaining to the change of frame in the ambient space $\tilde{\mathcal{E}}$. In fact, since here ν is a vector, say recorded by an observer $\mathcal{O}$; another observer, say $\mathcal{O}'$, registers a value $\nu' = Q\nu$, with $Q \in SO(3)$. The pertinent rates are then $\dot{\nu}$ and $\dot{\nu}' = Q\dot{\nu} + \dot{Q}\nu$, respectively. By writing $\dot{\nu}^*$ for $Q^{\mathrm{T}}\dot{\nu}'$, we get $\dot{\nu}^\diamond = \dot{\nu} + q\times\nu$, with q the characteristic vector of the skew-symmetric second-rank tensor $Q^{\mathrm{T}}\dot{Q}$. Consequently, by comparison with the general expression of $\nu^\diamond$ in Section 3.2, we get the explicit form of $\mathcal{A}(\nu)$ mentioned above.

We refer to gross deformation in terms of displacement field u, which is also called *phonon* field in the jargon of quasicrystal mechanics (see, e.g., Fan[34] and all references therein) because it is a natural descriptor for the propagation of elastic waves, while the word *phason* referred to the microstructural descriptor recalls that ν describes locally a rearrangement of atoms, that is, a possible change of the local symmetry phase.

As regards inertia, we have already claimed additive decomposition of bulk actions into inertial and non-inertial components. The former can be identified by imposing the equality between their power and the negative of kinetic energy for every choice of the rate fields involved (here $\dot{u}$) and $\dot{\nu}$. The presence of phason-type kinetic energy seems to be questionable (see, e.g., Schmicker and van Smaalen[45] and Rochal and Lorman[46]). For this reason, we write

$$\frac{\mathrm{d}}{\mathrm{d}t}\int_{\mathfrak{b}}\frac{1}{2}\rho\dot{u}^{\flat}\cdot\dot{u}\,\mathrm{d}x+\int_{\mathfrak{b}}\left(b^{in}\cdot\dot{u}+\beta^{in}\cdot\dot{\nu}\right)\mathrm{d}x=0, \tag{7}$$

with ρ the constant referential mass density and $\dot{u}^{\flat}$ the covector associated naturally with $\dot{u}$ by the metric in ambient space. Arbitrariness of $\dot{u}$ and $\mathfrak{b}$ implies the standard identification $b^{in}=-\rho\ddot{u}^{\flat}$, the right-hand side term being the rate of the macroscopic momentum, and $\beta^{\ddagger}\cdot\dot{\nu}=0$, which implies the possibility of rotational inertia, that is, for any vector $h\in\mathbb{R}^3$, a form for $\beta^{\ddagger}$ of the type $\beta^{\ddagger}\sim h\times\dot{\nu}$. A proposal in Mariano and Planas[39] is to identify h with $-\mathrm{curl}\dot{u}$. It is a physically motivated choice (see once again Mariano and Planas[39] for pertinent explanations) that is, in turn, a source of non-trivial analytical difficulties tackled in Bisconti and Mariano.[47]

We take the non-inertial component β to be *null* because we do not know any bulk action exerted directly from the environment on phason degrees of freedom. Perhaps exception could be attributed to the presence of radiative fields in extreme conditions, a case not yet investigated, as far as we know, and not considered here.

4.2.2 | Specific constitutive choices adopted here for computations

We consider orthonormal frames, so we do not distinguish between covariant and contravariant components of tensors. The duality pairing product indicated by a dot above coincides then with the standard scalar product.

We reduce the analysis to *small-strain regime* and consider linear constitutive setting for $\sigma\approx P$ and $\mathcal{S}_c\approx\mathcal{S}$. Precisely, we select

$$\sigma=\mathbb{C}Du+\mathbb{K}'D\nu,$$
$$S=\mathbb{K}'^{\mathrm{T}}Du+\mathbb{K}D\nu.$$

More specifically, in computations described below, we consider *two-dimensional samples*, with five-fold symmetry, so that the constitutive tensors take the explicit form

$$\mathbb{C}_{ijhk}=\lambda\delta_{ij}\delta_{hk}+\mu\left(\delta_{ih}\delta_{jk}+\delta_{ik}\delta_{jh}\right),$$
$$\mathbb{K}'_{ijhk}=k_1\delta_{ih}\delta_{jk}+k_2\left(\delta_{ij}\delta_{hk}-\delta_{ik}\delta_{jh}\right),$$
$$\mathbb{K}_{ijhk}=k_3\left(\delta_{i1}-\delta_{i2}\right)\left(\delta_{ij}\delta_{hk}-\delta_{ih}\delta_{jk}+\delta_{ik}\delta_{jh}\right),$$

where $i,j,h,k=1,2$; δ_{ij} is the Kronecker symbol, λ and μ are the Lamé constants, and k_1, k_2, and k_3 are constants characterizing the microstructural behavior; no summation is assumed over repeated indices in the last expression above.

As regards the phason self-action z, we presume here that it accounts just for dissipative effects inside each material element, so that in the decomposition $z=z^e+z^d$ we consider here (and just for the sake of simplicity), $z^e=0$ and

$$z^d=c\dot{\nu},$$

with c a positive constant. This choice is consistent with a proposal in Dubois[46]; for a more general constitutive structures for elastic quasicrystals, see Mariano and Planas.[39]

To assure non-negativity of the associated free energy density—a requirement of material stability—and that it vanishes over rigid-body motions, constitutive constants introduced above must satisfy the following bounds[48]:

$$\lambda+\mu>0,\ k_1>k_2,\ k_1+k_2+2\mu>\sqrt{(k_1+k_2-2\mu)^2+(4k_3)^2}.$$

For the sake of simplicity, we also neglect possible rotational inertia associated with phasons (a possibility mentioned above).

4.2.3 | Boundary conditions

We consider a mixed boundary value problem in small-strain regime (so that we write $\mathcal{B}$ for the domain in space considered but also use Cauchy's stress because we do not distinguish between reference and current shapes). We subdivide the body boundary $\partial\mathcal{B}$ into non-intersecting regions. We make two such choices. The first is $\partial\mathcal{B}^u \cup \partial\mathcal{B}^{\mathfrak{t}} = \partial\mathcal{B}$, where $\partial\mathcal{B}^u$ is a region where the displacement u (also called phonon field in the pertinent jargon) is prescribed, while $\partial\mathcal{B}^{\mathfrak{t}}$ sustains standard traction. The second choice deals with the phason field and is analogous. Namely, we write $\partial\mathcal{B}^\nu \cup \partial\mathcal{B}^\tau = \mathcal{B}$, where $\partial\mathcal{B}^\nu$ indicates where we (at least in principle) prescribe ν, and $\partial\mathcal{B}^\tau$ has the same meaning for τ. However, *we actually do not know any loading device able to assign ν and/or τ independently of the macroscopic deformation*. Consequently, our final choice of boundary conditions is as follows:

$$\begin{aligned} u &= \hat{u}, \ \ x \in \partial\mathcal{B}^u, \\ \nu &= 0, \ \ x \in \partial\mathcal{B}^\nu, \\ \sigma n &= \hat{\mathfrak{t}}, \ \ x \in \partial\mathcal{B}^{\mathfrak{t}}, \\ Sn &= 0, \ \ x \in \partial\mathcal{B}^\tau, \end{aligned}$$

where $\hat{u}$ and $\hat{\mathfrak{t}}$ are prescribed values of u and $\mathfrak{t}$, respectively.

5 | FINITE ELEMENT SCHEME

We select test fields δu and $\delta\nu$ both in $H^1(\mathcal{B})$. They vanish on $\partial\mathcal{B}^u$ and $\partial\mathcal{B}^\nu$) respectively. Equation (6) allows us to write

$$\begin{aligned} \int_{\mathcal{B}} D\delta u \cdot \sigma \mathrm{d}x + \int_{\mathcal{B}} D\delta\nu \cdot S \mathrm{d}x - \int_{\mathcal{B}} \delta\nu \cdot z \mathrm{d}x = \int_{\mathcal{B}} \delta u \cdot \rho\ddot{u} \mathrm{d}x \\ + \int_{\mathcal{B}} \delta u \cdot b \mathrm{d}x + \int_{\partial\mathcal{B}^{\mathfrak{t}}} \delta u \cdot \mathfrak{t} \mathrm{d}\mathcal{H}^2 + \int_{\partial\mathcal{B}^\tau} \delta\nu \cdot \tau \mathrm{d}\mathcal{H}^2, \end{aligned}$$

where we use the standard volume measure for the sake of simplicity and write $\mathrm{d}\mu(x) = \mathrm{d}x$.

With $\mathbf{U}$ and $\mathbf{V}$ the vectors collecting nodal values of u and ν, which we write as $\mathbf{u}$ and ν in column form, respectively, we write interpolations in space as follows:

$$\mathbf{u}(x,t) = \mathbf{N}_u(x)\mathbf{U}(t), \quad \nu(x,t) = \mathbf{N}_\nu(x)\mathbf{V}(t),$$

with $\mathbf{N}_u$ and $\mathbf{N}_\nu$ matrices of shape functions. For test fields, we choose the same form:

$$\delta\mathbf{u}(x,t) = \mathbf{N}_u(x)\delta\mathbf{U}(t), \quad \delta\nu(x,t) = \mathbf{N}_\nu(x)\,\delta\mathbf{V}(t).$$

Consequently, the weak balance above writes in matrix form as

$$\begin{bmatrix} \mathbf{M}_{uu} & \mathbf{0} \\ \mathbf{0} & \mathbf{0} \end{bmatrix} \begin{bmatrix} \ddot{\mathbf{U}} \\ \ddot{\mathbf{V}} \end{bmatrix} + \begin{bmatrix} \mathbf{0} & \mathbf{0} \\ \mathbf{0} & \mathbf{D}_{\nu\nu} \end{bmatrix} \begin{bmatrix} \dot{\mathbf{U}} \\ \dot{\mathbf{V}} \end{bmatrix} + \begin{bmatrix} \mathbf{K}_{uu} & \mathbf{K}_{u\nu} \\ \mathbf{K}_{u\nu}^{\mathrm{T}} & \mathbf{K}_{\nu\nu} \end{bmatrix} \begin{bmatrix} \mathbf{U} \\ \mathbf{V} \end{bmatrix} = \begin{bmatrix} \mathbf{F}_u(t) \\ \mathbf{F}_\nu(t) \end{bmatrix},$$

where, with $\mathfrak{b}$ the single finite element,

$$\mathbf{M}_{uu} = \int_{\mathfrak{b}} \mathbf{N}_u^{\mathrm{T}} \rho \mathbf{N}_u \mathrm{d}x,$$

$$\mathbf{D}_{\nu\nu} = \int_{\mathfrak{b}} (\mathbf{N}_\nu)^{\mathrm{T}} c \mathbf{N}_\nu \mathrm{d}x.$$

$$\mathbf{K}_{uu} = \int_{\mathfrak{b}} (D\mathbf{N}_u)^{\mathrm{T}} \boldsymbol{C}\, (D\mathbf{N}_u)\, \mathrm{d}x,$$

$$\mathbf{K}_{uv} = \int_{\mathfrak{b}} (D\mathbf{N}_u)^{\mathrm{T}} \boldsymbol{K}' (D\mathbf{N}_v)\, \mathrm{d}x,$$

$$\mathbf{K}_{vv} = \int_{\mathfrak{b}} (D\mathbf{N}_v)^{\mathrm{T}} \boldsymbol{K} (D\mathbf{N}_v)\, \mathrm{d}x,$$

$$\mathbf{F}_u = \int_{\mathfrak{b}} \mathbf{N}_u^{\mathrm{T}} \mathbf{b} \mathrm{d}x + \int_{\partial\mathfrak{b}} \mathbf{N}_u^{\mathrm{T}} \mathbf{t} \mathrm{d}\mathcal{H}^2,$$

$$\mathbf{F}_v = \int_{\partial\mathfrak{b}} \mathbf{N}_v^{\mathrm{T}} \tau \mathrm{d}\mathcal{H}^2.$$

with $\mathbf{b}$ and $\mathbf{t}$ the column counterparts of b and $\mathfrak{t}$.

In the two-dimensional setting considered in the computations we develop here, matrices $\boldsymbol{C}$, $\boldsymbol{K}$, and $\boldsymbol{K}'$ are given by

$$\boldsymbol{C} = \begin{bmatrix} \lambda + 2\mu & 0 & 0 & \lambda \\ 0 & \mu & \mu & 0 \\ 0 & \mu & \mu & 0 \\ \lambda & 0 & 0 & \lambda + 2\mu \end{bmatrix},$$

$$\boldsymbol{K}' = \begin{bmatrix} k_3 & 0 & 0 & k_3 \\ 0 & -k_3 & k_3 & 0 \\ 0 & -k_3 & k_3 & 0 \\ -k_3 & 0 & 0 & -k_3 \end{bmatrix},$$

$$\boldsymbol{K} = \begin{bmatrix} k_1 & 0 & 0 & k_2 \\ 0 & k_1 & -k_2 & 0 \\ 0 & -k_2 & k_1 & 0 \\ k_2 & 0 & 0 & k_1 \end{bmatrix}.$$

In the same setting, the column vectors appearing in the equations above are explicitly

$$\mathbf{u} = \begin{bmatrix} u_1 \\ u_2 \end{bmatrix}, \qquad v = \begin{bmatrix} v_1 \\ v_2 \end{bmatrix},$$

$$D\mathbf{u} = \begin{bmatrix} \partial_1 u_1 \\ \partial_2 u_1 \\ \partial_1 u_2 \\ \partial_2 u_2 \end{bmatrix}, \qquad Dv = \begin{bmatrix} \partial_1 v_1 \\ \partial_2 v_1 \\ \partial_1 v_2 \\ \partial_2 v_2 \end{bmatrix},$$

$$\sigma = \begin{bmatrix} \sigma_{11} \\ \sigma_{12} \\ \sigma_{21} \\ \sigma_{22} \end{bmatrix}, \qquad \mathbf{S} = \begin{bmatrix} S_{11} \\ S_{12} \\ S_{21} \\ S_{22} \end{bmatrix},$$

$$\mathbf{t} = \begin{bmatrix} \mathfrak{t}_1 \\ \mathfrak{t}_2 \end{bmatrix}, \qquad \tau = \begin{bmatrix} \tau_1 \\ \tau_2 \end{bmatrix},$$

$$\mathbf{b} = \begin{bmatrix} b_1 \\ b_2 \end{bmatrix}.$$

6 | ANALYSES

6.1 | Preliminaries

Table 1 summarizes the values of the constitutive coefficients considered in the analyses.

TABLE 1 Numerical values of the constitutive coefficients (see other studies[49–51])

Lamé constants	λ	0.75×10^{11}	N/m^2
	μ	0.65×10^{11}	N/m^2
Phason elastic constants	k_1	0.81×10^{11}	N/m^2
	k_2	-0.42×10^{11}	N/m^2
Phonon–phason coupling constant (ratio to k_1)	k_3/k_1	0.1	
Mass density	ρ	5100	kg/m^3
Phason friction	c	exp 18, exp 23	$N/(m/s)/m^3$

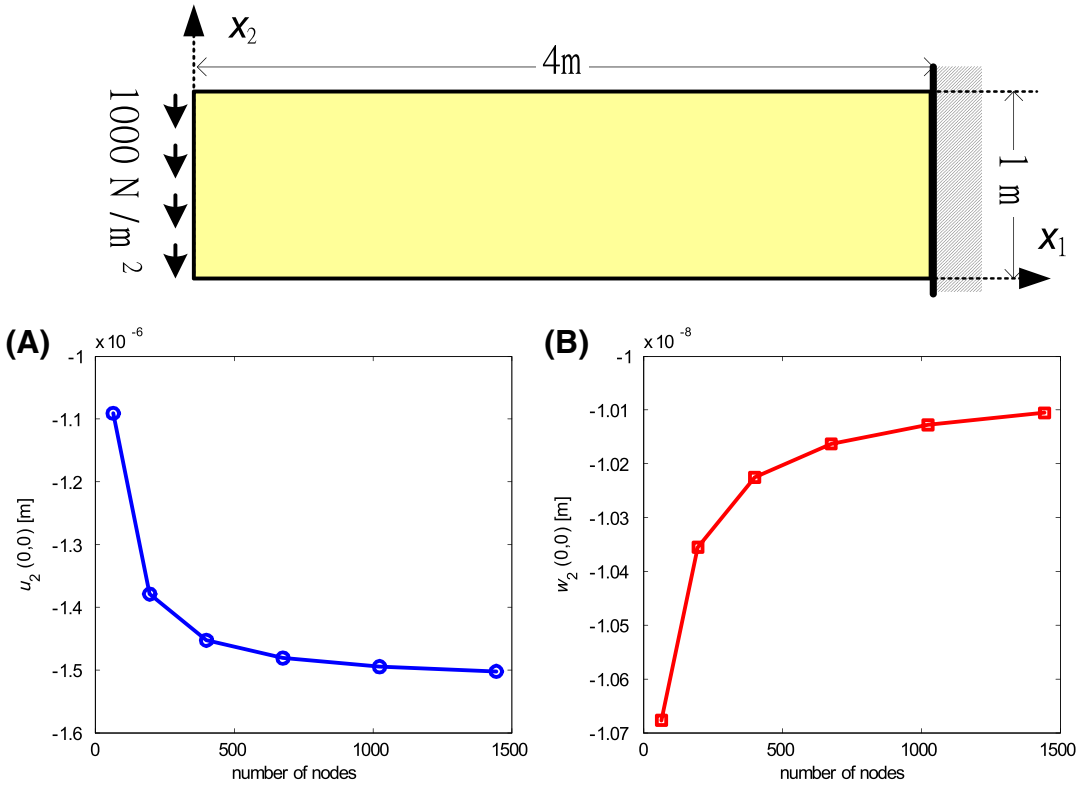

FIGURE 1 (A,B) Cantilever beam under static load: numerical convergence of displacement and phason field

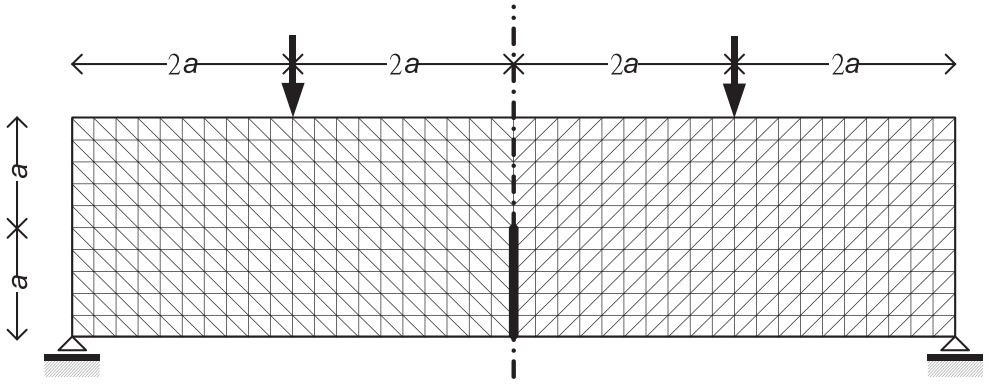

FIGURE 2 Scheme for static analyses with incremental loading

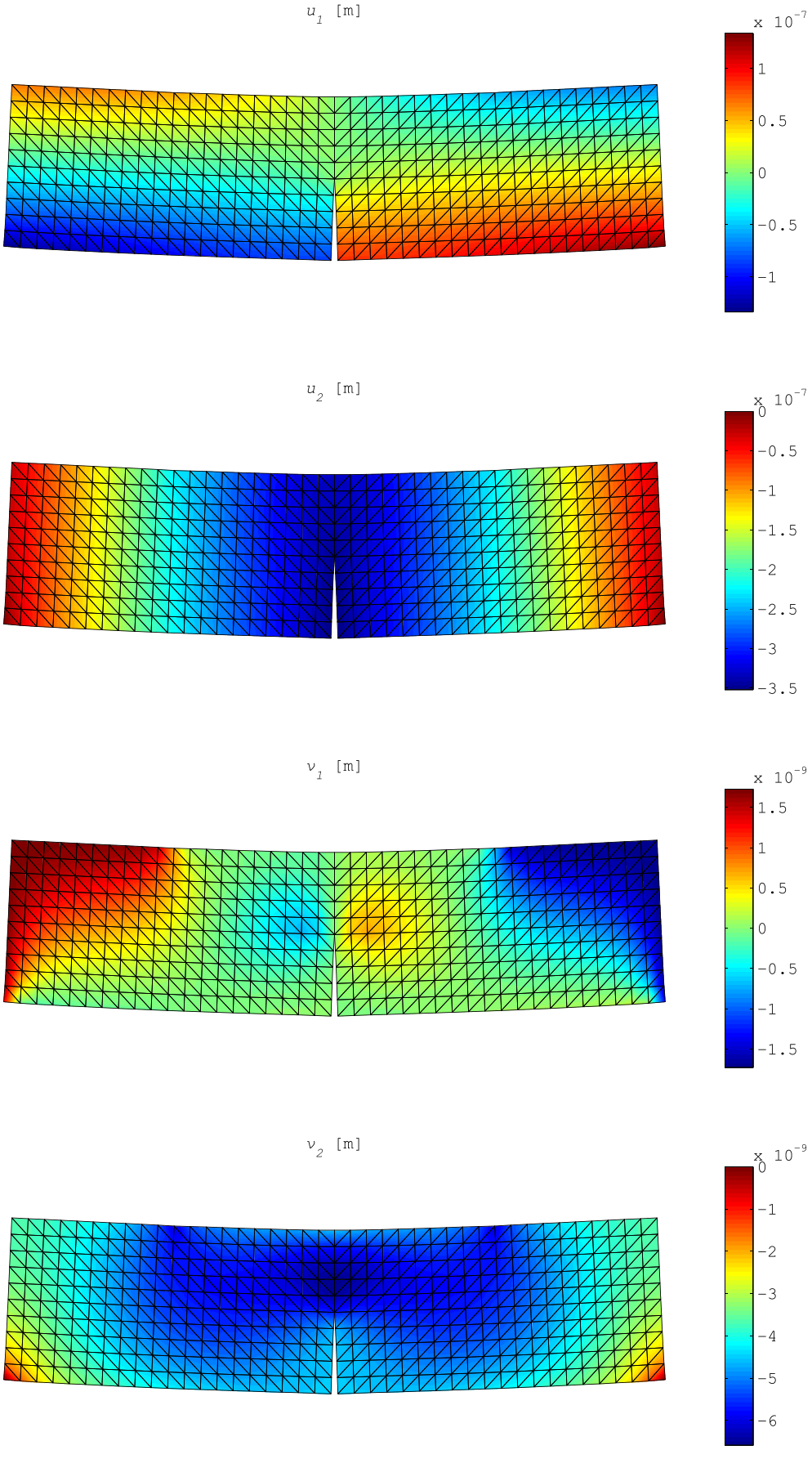

FIGURE 3 Displacement and phason field for the four-point bending test. Values magnified by a factor equal to 5×10^5

We test the finite element scheme by checking numerical convergence in the case of a simple cantilever beam under a static load uniformly distributed at one end, as depicted in Figure 1. Statics implies a reduction of the numerical scheme to

$$\begin{bmatrix} \mathbf{K}_{uu} & \mathbf{K}_{uv} \\ \mathbf{K}_{uv}^{\mathrm{T}} & \mathbf{K}_{vv} \end{bmatrix} \begin{bmatrix} \mathbf{U} \\ \mathbf{V} \end{bmatrix} = \begin{bmatrix} \mathbf{F}_u \\ \mathbf{F}_v \end{bmatrix},$$

with $\mathbf{F}_v = \mathbf{0}$ along the external body boundary.

6.2 | Static analysis: Phason localization around a crack tip

Looking always at the previous static setting, we consider a four-point bending test of a notched beam, as depicted in Figure 2.

We consider a characteristic dimension of the beam $a = 1.0\,\mathrm{m}$ and a unit thickness (1.0 m). The load is $F = 1000\,\mathrm{N}$. We neglect body forces ($b = 0$). We adopt a structured mesh for the sake of simplicity, as the wavelet analysis presented in the following sections requires that the data be organized over a regular grid. We consider two different mesh levels: one of grid dimension equal to $a/25$—and we use it for the static analysis—and a coarser mesh with grid dimension equal to $a/5$ (the one represented in Figure 2), which is adopted for the dynamic analyses described in the following section.

Such an analysis evidences localization of the phason field around the crack tip (Figure 3). This type of phenomenon occurs also in other types of materials with vector-type representation of the material microstructure.[10]

6.3 | Dynamic setting

Under the same beam, we consider an impulsive load controlled by the function $\lambda(t)$ described in Figure 4.

As initial conditions, we assume

$$u(x,0) = 0; \quad \dot{u}(x,0) = 0; \quad v(x,0) = 0; \quad \dot{v}(x,0) = 0.$$

Impulse duration is $t_{imp} = 0.125{\times}10^{-3}$. We have chosen such a value considering that the time necessary for a compression sound wave to travel across the sample height ($= 2a = 2.0\,\mathrm{m}$) would be of $0.35 \times 10^{-3}\,\mathrm{s}$ if the sample would be made of a simple body with Young's modulus $E = \frac{\mu(3\lambda+2\mu)}{\lambda+\mu}$, Lamé constants from Table 1, so that the wave speed would be $v \simeq \sqrt{\frac{E}{\rho}} \simeq 5700\,\mathrm{m/s}$, with ρ value once again from Table 1.

Simulation duration is $T = 5.0 \times 10^{-3}s$. For it, we adopt a Newmark scheme with pure trapezoidal rule and a time step $\Delta t = 2.0 \times 10^{-6}\,\mathrm{s}$. We consider two values of the phason friction coefficient: $c = \exp(18)\,\mathrm{N/(m/s)/m^3}$ and $c = \exp(23)\,\mathrm{N/(m/s)/m^3}$. Pertinent snapshots at $0.1 \times 10^{-3}\,\mathrm{s}$ are shown in Figure 5. The discrepancy between displacement and phason field, above all around geometric (crack tip) and load discontinuities is visually evident. Wavelets furnish us a more detailed analysis.

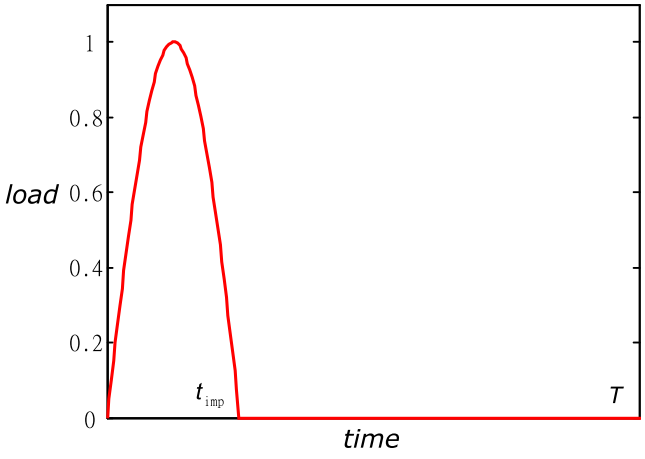

FIGURE 4 Load multiplier $\lambda(t)$

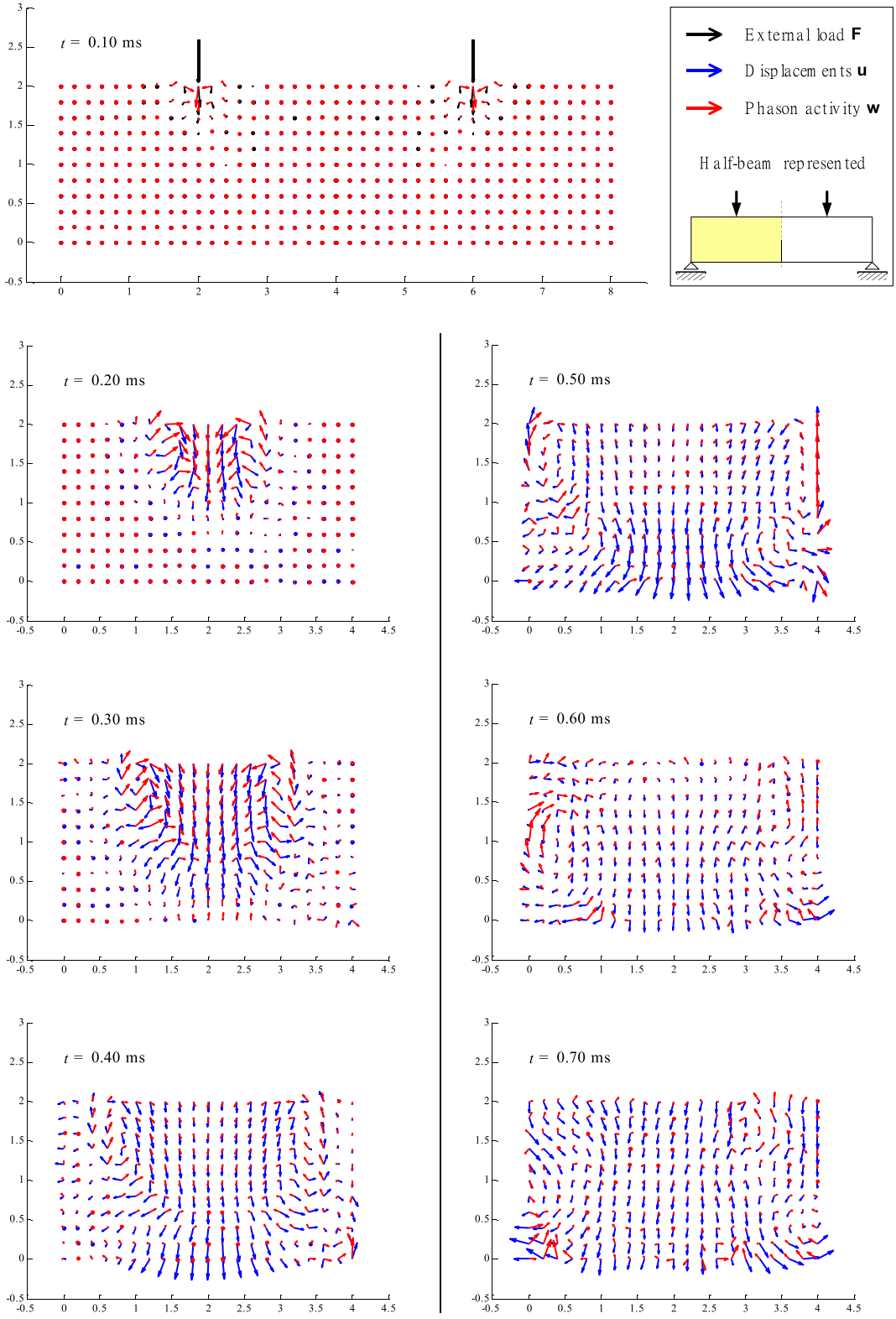

FIGURE 5 Snapshots at 0.1×10^{-3} s under impulsive loading

6.4 | Wavelet analyses

We apply wavelets (in space and time) along two sections of the beam, those indicated in Figure 6. The touch points where geometric and load discontinuities are located.

FIGURE 6 Sections involved in wavelet analysis

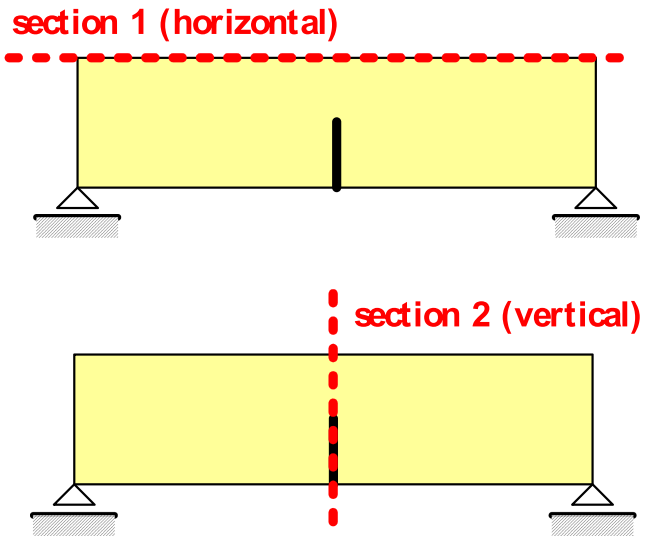

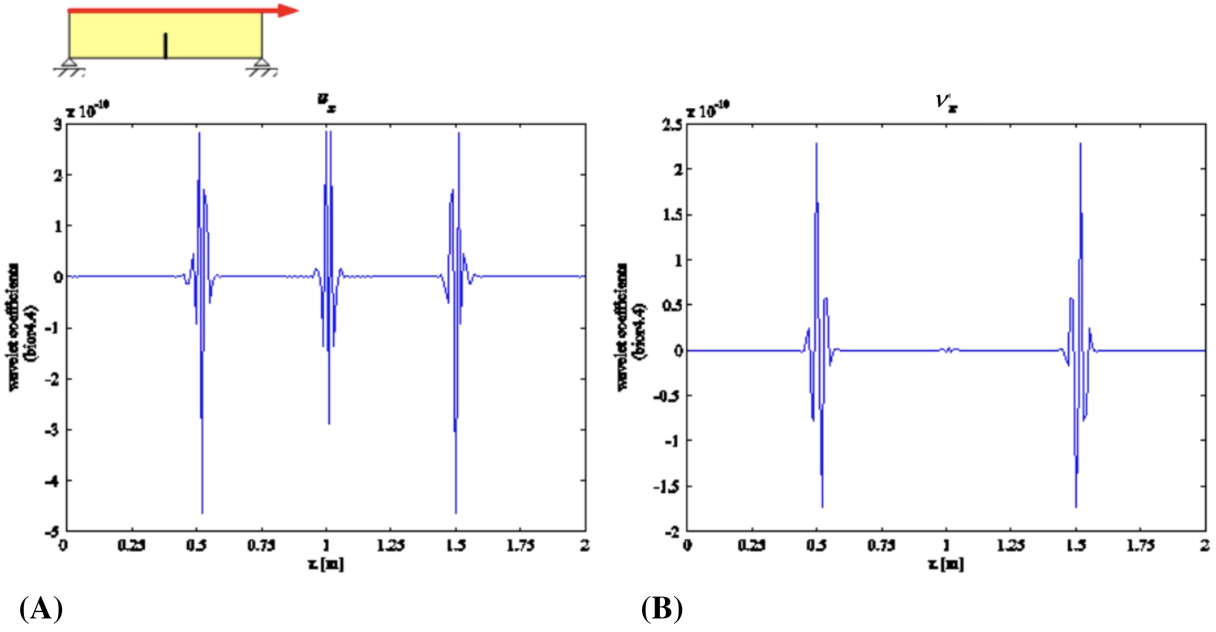

(A) (B)

FIGURE 7 Wavelet coefficients along Section 1: (A) displacement, (B) phason field

6.4.1 | Static data

In the static case, the analysis in terms of wavelets refers just to space variables. This type of analysis can be used to identify singularities.

Wavelets coefficients pertaining to the two sections appear in Figures 7–9.

First we refer to biorthogonal wavelets. They produce small coefficients in domains of regularity for the fields considered and higher coefficients when singularities occur, so that they are well suited for singularity detection.

As shown in Figure 7, the analysis in terms of biorthogonal wavelets for the displacement field along Section 1 in Figure 6 reveals that u receives a direct crack tip influence over the boundary. This is not so for phasons v, which suffer just the influence of applied load power conjugated with u, as evidenced in Panel (B) of the same figure.

Wavelets offer different descriptive possibilities. This is evident in the analysis along Section 2. In Panel (A) of Figure 8, we see how biorthogonal wavelets allow just to detect the most critical point (let us say) of a geometric discontinuity. The wavelet coefficients evidence just the crack tip. At variance, the Haar wavelets, applied to the analysis of u, individualize the whole crack path, as shown in Panel (B) of the same figure. Such a difference does not clearly appear when we analyze the field $\tilde{v}$ along Section 2, as shown in Figure 9. The reason is that phasons are mainly localized around the crack tip and

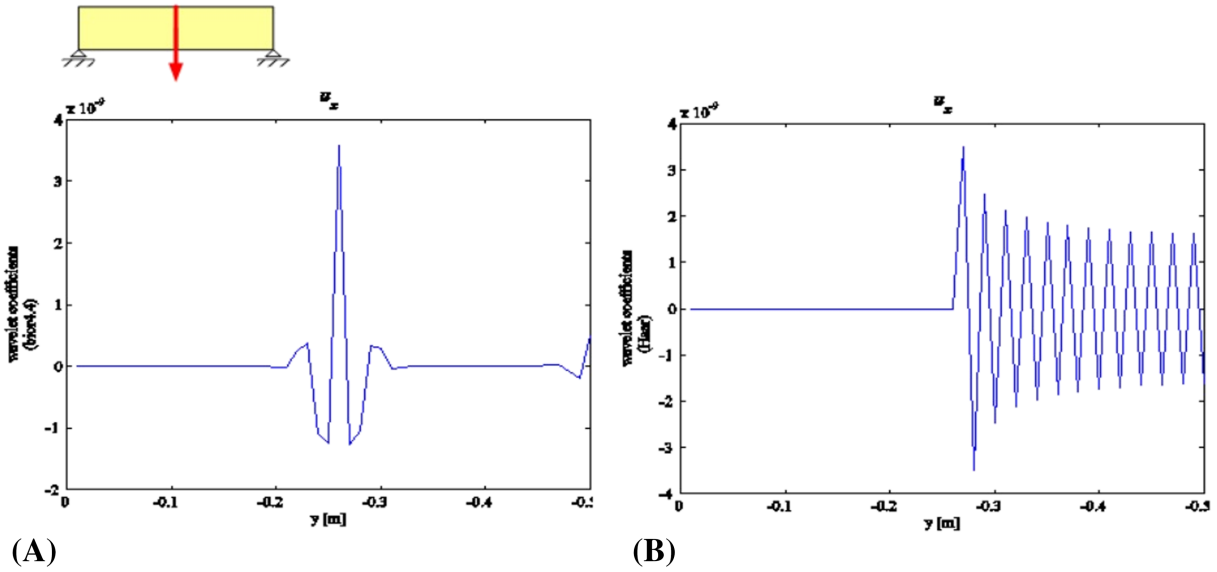

FIGURE 8 Wavelet coefficients of the displacement along Section 2: (A) biorthogonal wavelet detects crack tip; (B) the Haar wavelet evidences the whole crack

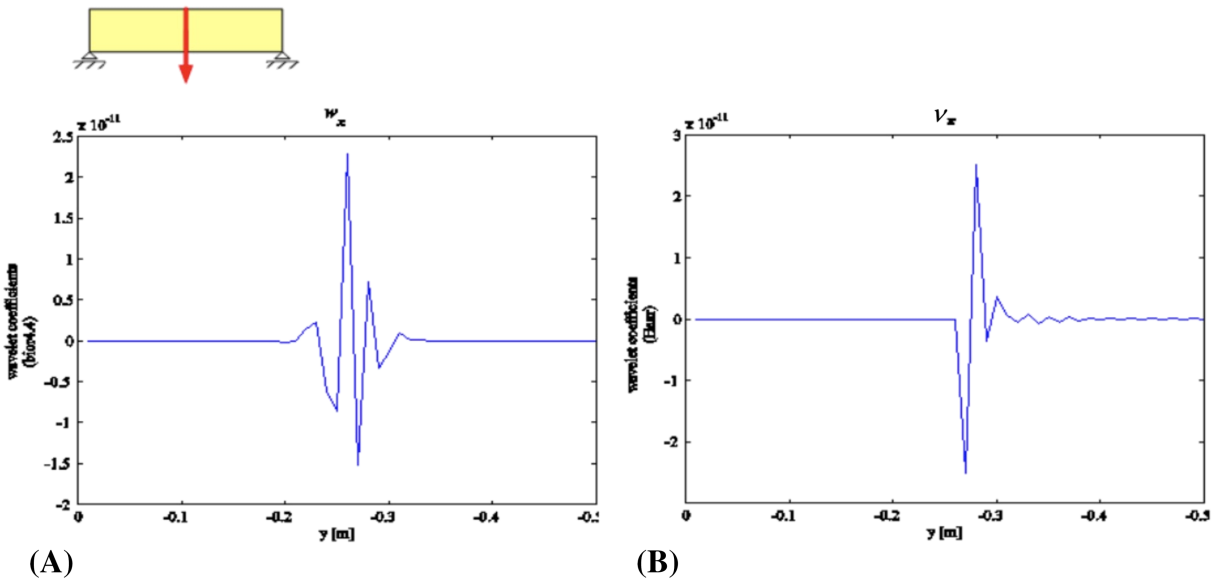

FIGURE 9 Wavelet coefficients of the phason field along Section 2: (A) biorthogonal wavelet, (B) the Haar wavelet. Both choices allow us to detect only the crack tip for this field because phasons are localized there

do not receive a prominent influence from crack edges. Consequently, if we think of a monitoring process, the use of the Haar wavelets helps us in detecting localization of fields around known geometric discontinuities.

Notice that we have used different scales in the figures. Wavelet coefficients of u are 10 times smaller than those of v. Also, coefficients of the wavelet transform of v along Section 2 are 10 times bigger than the ones along Section 1.

6.4.2 | Dynamic data

In the dynamic case, we use wavelets referring to both time and space variables.

We first consider a friction coefficient value $c = \exp(23)\,\mathrm{N/(m/s)m^3}$. Wavelet coefficients of u show that the perturbation induced by applied load and crack (the counterparts of those described in Figure 7 for the static setting) do not remain localized and tend to disappear in time. A few large spikes initially present evolve into several smaller spikes distributed along the section considered (Figure 10A).

The effects shown in Figure 7B, do not propagate in time under an impulsive load (Figure 10B). Just after load application, wavelet coefficients decrease and remain localized, due to the presence of phason friction.

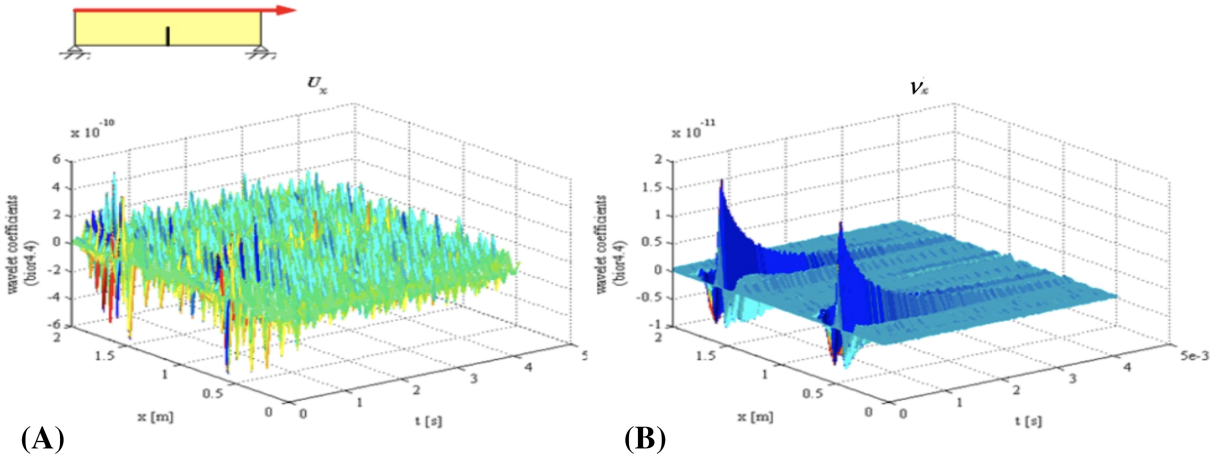

FIGURE 10 Time histories of wavelet coefficients u (A) and v (B) along Section 1. $c = \exp(23)$ N/(m/s)m^3

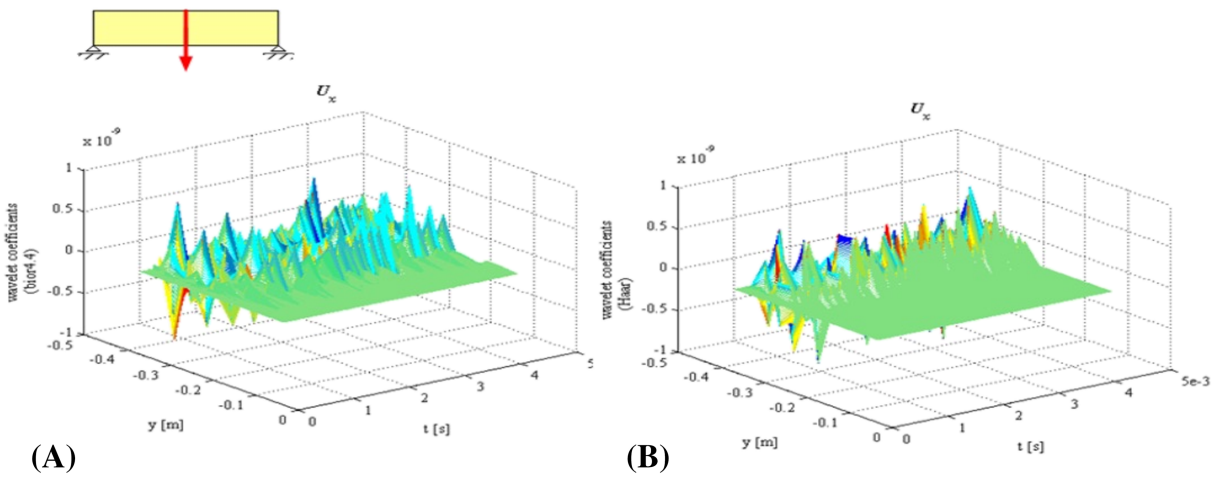

FIGURE 11 Time histories of wavelet coefficients of u along Section 2. Panel (A): biorthogonal wavelet. Panel (B): the Haar wavelet. $c = \exp(23)$ N/(m/s)m^3

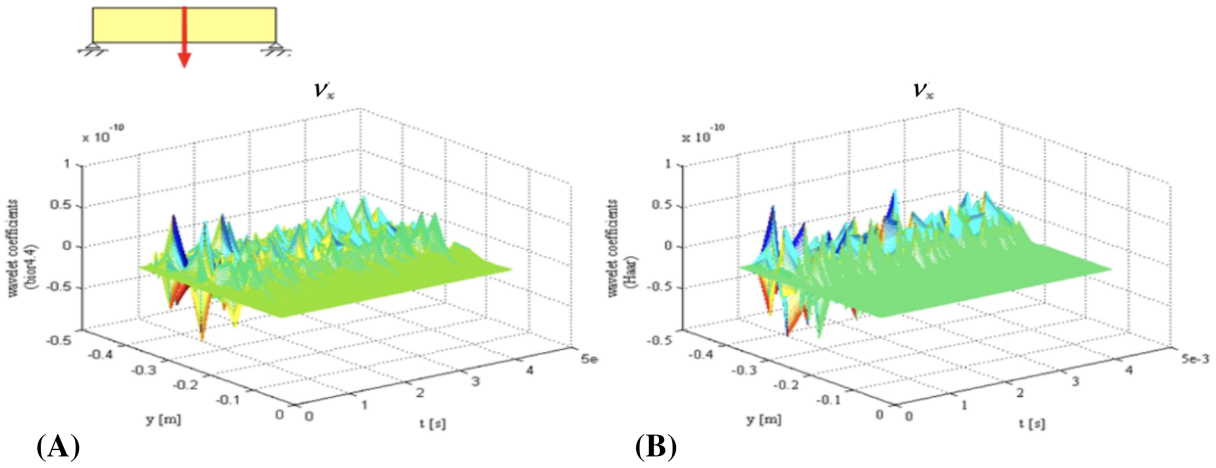

FIGURE 12 Time histories of wavelet coefficients of v along Section 2. Panel (A): biorthogonal wavelet. Panel (B): the Haar wavelet. $c = \exp(23)$ N/(m/s)m^3

Analyses along Section 2 indicate how the crack influences in the same way, for a qualitative point of view, wavelet coefficients in both displacement (Figure 11) and phason field (Figure 12), with both the biorthogonal and Haar wavelets.

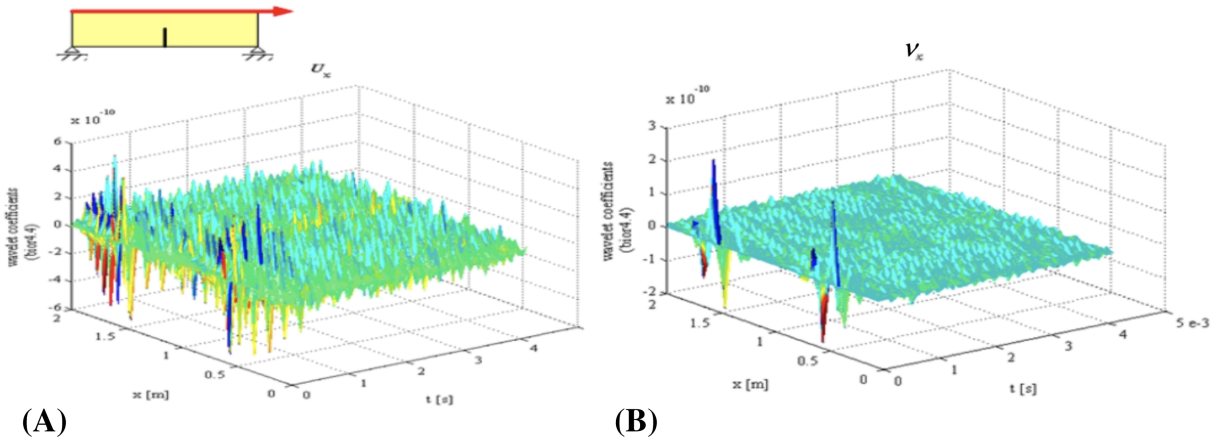

FIGURE 13 Time histories of biorthogonal wavelet coefficients of u (Panel A) and v (Panel B) along Section 2. $c = \exp(18)$ N/(m/s)m^3

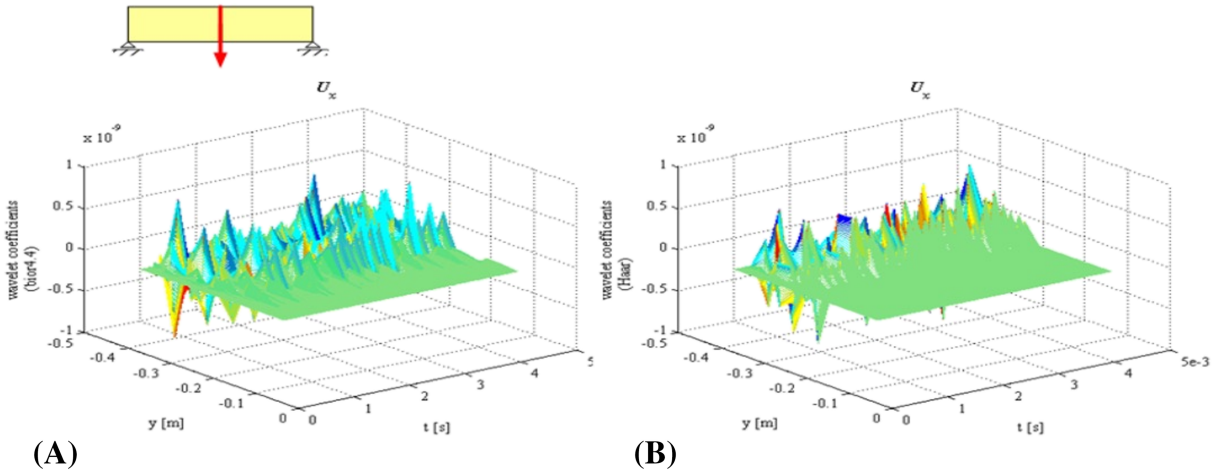

FIGURE 14 Time histories of u along Section 2. Panel (A): analysis in terms of biorthogonal wavelets. Panel (B): analysis in terms of the Haar wavelets. $c = \exp(18)$ N/(m/s)m^3

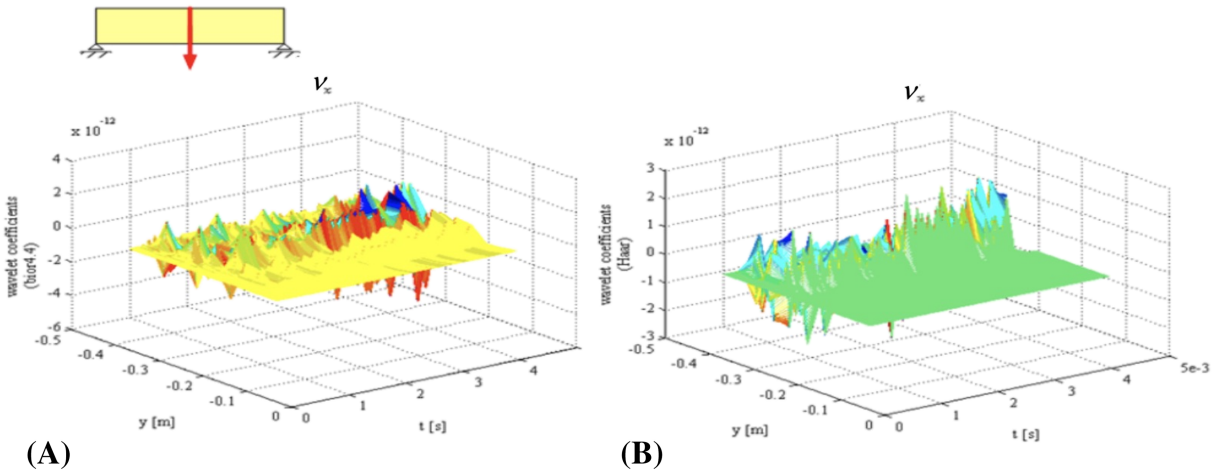

FIGURE 15 Time histories of v along Section 2. Panel (A): analysis in terms of biorthogonal wavelets. Panel (B): analysis in terms of the Haar wavelets. $c = \exp(18)$ N/(m/s)m^3

Since experimental values of c seem to be not available with certainty (and the same situation affects the coupling coefficient here fixed at $0.1k_1$), we have performed parametric analyses by varying c. Here we report and compare just the results for $c = \exp(18)\,\mathrm{N/(m/s)m^3}$ A comparison between Figures 10A and 13A shows a scarce influence on u. We find the same large localized peaks, which propagate in time.

At variance, by comparing Figures 10B and 13B, we see how lower friction allows a propagation of perturbations along the section considered, while with $c = \exp(23)\,\mathrm{N/(m/s)m^3}$ load effects remain well localized. When $c = \exp(18)\,\mathrm{N/(m/s)m^3}$, load effects are characterized by smaller wavelet coefficients uniformly distributed along the section. Also, in this case, the qualitative behavior of v is similar to the one of u.

Analyses along Section 2 (see Figures 14–16) reveal once again the influence of friction coefficient variation mainly on the phason field: while wavelet coefficients associated with u are of the same order in both friction coefficient values considered (Figures 12 and 15), those associated to v in Figure 13 are two order smaller of those in Figure 16. Results obtained by the Haar and biorthogonal wavelets do not differ prominently.

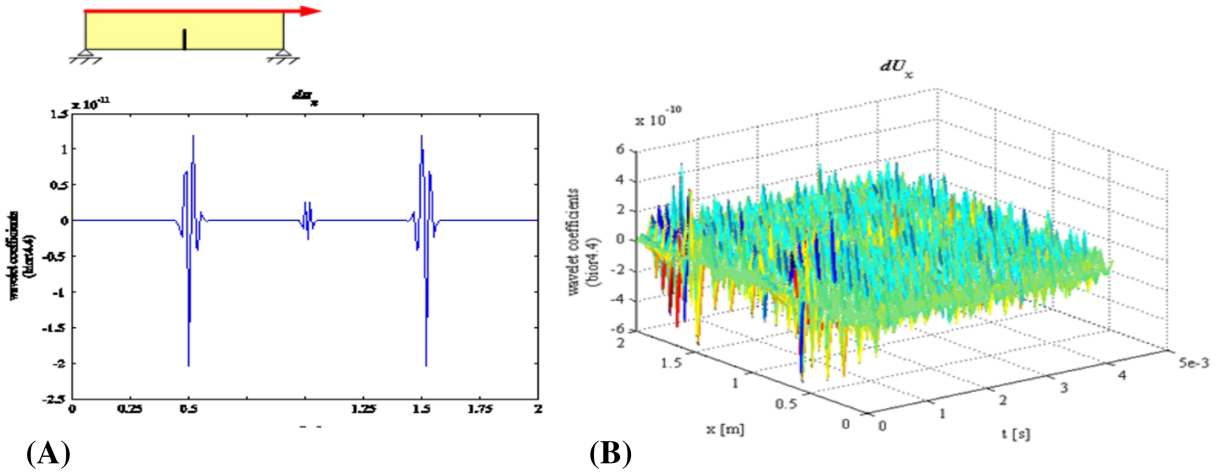

FIGURE 16 Variations of u along Section 1 between considering and not considering phasons. Panel (A): static setting. Panel (B): dynamics (biorthogonal wavelets). $c = \exp(18)\,\mathrm{N/(m/s)m^3}$

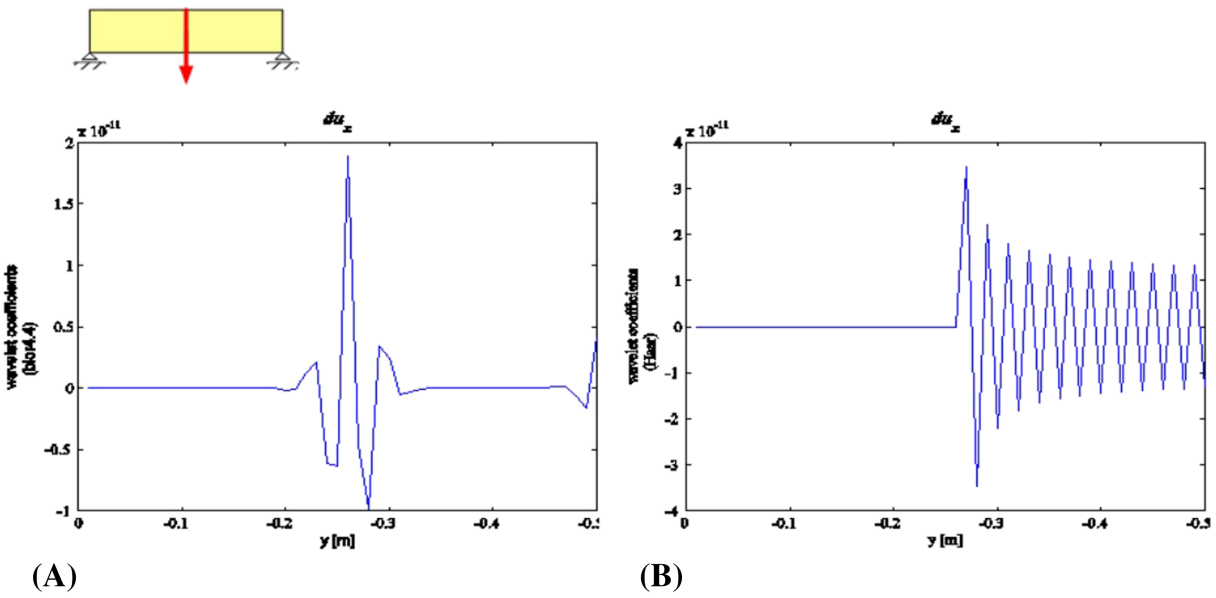

FIGURE 17 Variations of u along Section 2 between considering and not considering phasons in statics. Panel (A): biorthogonal wavelets. Panel (B): the Haar wavelets

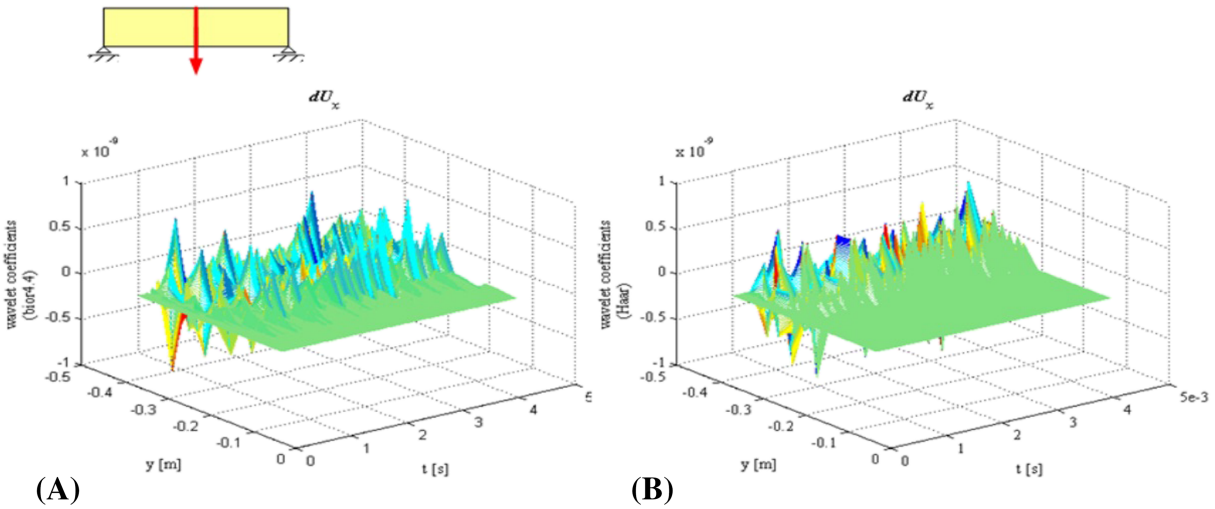

FIGURE 18 Variations of u along Section 2 between considering and not considering phasons in dynamics. Panel (A): biorthogonal wavelets. Panel (B): the Haar wavelets. $c = \exp(18)\,\mathrm{N/(m/s)m^3}$

6.4.3 | When we do not consider phasons: Comparison with a simple body

What changes if we neglect phasons and consider a quasicrystal as a simple body, assigning it just the experimental values of the Lamé constants listed in Table 1? Answering this gives indications for a more general question on the appropriateness of describing simple bodies in terms of the multi-field scheme summarized in Section 3.

To better estimate the microstructural effects, we repeat the analyses described above, by neglecting phasons. Then, we compare results with those including phasons and the lowest phason friction value, that is, $c = \exp(18)\,\mathrm{N/(m/s)m^3}$, among those considered in previous computations.

We report in Figures 16–18 differences between the two cases (and we indicate by some abuse of notation such differences by du and dv in the graphs), in both static and dynamic cases, by considering always Sections 1 and 2 in the sample structure analyzed so far.

Figure 16 refers to the static setting and Section 1. We see how considering phasons influences u in both the points where loads are applied and the middle point, which belong to the vertical line including the crack. When we refer to dynamics (Figure 17), we see that such influence remains in time and is not negligible.

Figures 17 and 18 refer to Section 2. Both biorthogonal and the Haar wavelets identify differences between considering and neglecting phasons (Figure 17). The effect is more evident in dynamics (Figure 18). There is also something more: in finite element analyses, we have noticed that phasons localize around the crack tip and seem to be indifferent to crack edges. The wavelet analysis (Figures 17 and 18) shows how phasons have an indirect influence on u along crack edges.

7 | ADDITIONAL REMARKS

The procedure we have suggested here can be interpreted in two ways:

(1) Wavelets can be used in a post-processing protocol after finite-element-type analyses on mechanical processes. In this sense, they may help, as in the case of quasicrystals shown here, in developing a detailed characterization of across-scale interactions in complex materials.
(2) In the case we have at disposal data emerging from experiments (let us say essentially in dynamic setting), wavelets may be used in a monitoring protocol for they are able to individualize geometric discontinuities, which can be a source of material instabilities and failure.

What we proposed in this paper is naturally open to further developments. Specifically, it might be referred to stress-based dual computational schemes (as those in Bruggi and Venini[52]), extended finite element method (X-FEM) adapted to the multi-field scheme (as done in Mariano and Stazi[16]), also variational integrators in the same setting (as those discussed in Focardi and Mariano[19]).

ACKNOWLEDGEMENTS

This work belongs to activities of the research group "Theoretical Mechanics" in the "Centro di Ricerca Matematica Ennio De Giorgi" of the Scuola Normale Superiore in Pisa.

CONFLICTS OF INTEREST

This work does not have any conflicts of interest.

ORCID


Paolo Maria Mariano https://orcid.org/0000-0002-3841-8408

REFERENCES

1. Truesdell CA, Noll W. The non-linear field theories of mechanics. *Handbuch der Physik*. Berlin: Springer-Verlag; 1965:Band III/3 1-602.
2. Truesdell CA, Toupin RA. Classical field theories of mechanics. *Handbuch der Physik*. Berlin: Springer-Verlag; 1960:Band III/1 226-793.
3. Šilhavý M. *The Mechanics and Thermodynamics of Continuous Media*. Berlin: Springer-Verlag; 1997.
4. Capriz G. *Continua with Microstructure*. Berlin: Springer Verlag; 1989.
5. Mariano PM. Multifield theories in mechanics of solids. *Adv Appl Mech*. 2002;38:1-93.
6. Mariano PM. Mechanics of material mutations. *Adv Appl Mech*. 2014;XX:1-92.
7. Focardi M, Mariano PM, Spadaro EN. Multi-value microstructural descriptors for complex materials: analysis of ground states. *Arch Rational Mech Anal*. 2015;215:899-933.
8. Mariano PM, Modica G. Ground states in complex bodies. *ESAIM: Control Optim Calc Var*. 2009;15:377-402.
9. Khurana A, Bala S, Khan H, Tomar SK, Neff P. On the dispersion of waves for the linear thermoelastic relaxed micromorphic model. *J Thermal Stresses*. 2020;43:3-20.
10. Mariano PM, Stazi FL. Strain localization in elastic microcracked bodies. *Comp Meth Appl Mech Eng*. 2001;190:5657-5677.
11. Nag S, Junge T, Curtin WA. Atomistic-continuum coupling of random alloys. *Mod Sim Mat Sci Eng*. 2019;27:075004.
12. Beex LAA, Peerlings RHJ, Geers MGD. A quasicontinuum methodology for multiscale analyses of discrete microstructural models. *Int J Num Meth Eng*. 2011;87:701-718.
13. Beex LAA, Peerlings RHJ, Geers MGD. A multiscale quasicontinuum method for lattice models with bond failure and fiber sliding. *Comp Meth Appl Mech Eng*. 2014;269:108-122.
14. Miehe C, Aldakheel F, Teichtmeister S. Phase-field modeling of ductile fracture at finite strains: a robust variational-based numerical implementation of a gradient-extended theory by micromorphic regularization. *Int J Num Meth Eng*. 2017;111:816-863.
15. Miehe C, Teichtmeister S, Aldakheel F. Phase-field modelling of ductile fracture: a variational gradient-extended plasticity-damage theory and its micromorphic regularization. *Phil Trans Royal Soc*. 2016;374:20150170.
16. Mariano PM, Stazi FL. Strain localization due to crack–microcrack interactions: X-FEM for a multifield approach. *Comp Meth Appl Mech Eng*. 2004;193:5035-5062.
17. Marsden JE, Patrick GW, Shköller S. Geometry, variational integrators and nonlinear PDEs. *Comm Math Phys*. 1998;199:351-395.
18. Marsden JE, West M. Discrete mechanics and variational integrators. *Acta Num*. 2001;10:357-514.
19. Focardi M, Mariano PM. Discrete dynamics of complex bodies: variational integrators and convergence. *Discr Cont Dyn Sys - B*. 2009;11:109-130.
20. Bosi A. Early-Warning Monitoring System for Masonry Structures. *PhD Thesis*: University of Florence Italy, and TU Braunschweig Germany; 2008.
21. Bosi A, Mollaioli F, Mariano PM. Wavelet analysis on detecting pulse-like earthquakes. *AIP Conf Proc*. 2008;1020:1803-1810.
22. Mollaioli F, Bosi A. Wavelet analysis for the characterization of forward-directivity pulse-like ground motions on energy basis. *Meccanica*. 2012;47:203-219.
23. Whitney R. Synthetic pulse model for near-fault effects on structures. *Pract Period Struct Des Constr*. 2020;25:04020013.
24. Sinambela M, Tarigan K, Humaidi S, Situmorang M. Wavelet based machine learning approach for spectral seismic signal analysis: a case study North Tapanuli earthquake. *AIP Conf Proc*. 2020;2221:0600011.
25. Shechtman D, Blech I, Gratias D, Cahn JW. Metallic phase with long-range orientational order and no translational symmetry. *Phys Rev Lett*. 1984;53:1951-1954.
26. Dubois J-M. *Useful Quasicrystals*. Singapore: World Scientific; 2005.
27. Mallat S. *A Wavelet Tour on Signal Processing*. New York: Academic Press; 1998.
28. Ericksen JL, Truesdell CA. Exact theory of stress and strain in rods and shells. *Arch Rational Mech Anal*. 1958;1:295-323.
29. Mariano PM. Trends and challenges in the mechanics of complex materials: a view. *Phil Trans Royal Soc London A*. 2016;374:31. 20150341.
30. Mariano PM. Mechanics of quasi-periodic alloys. *J Nonlinear Sci*. 2006;16:45-77.

31. International Union of Crystallography. Report of the Executive Committee for 1991. *Acta Cryst*. 1992;A48:922-946.
32. Bindi L, Steinhardt PJ, Yao N, Lu PJ. Natural quasicrystals. *Science*. 2009;324:1306-1309.
33. Ding D-H, Yang W, Hu C, Wang R. Generalized theory of quasicrystals. *Phys Rev B*. 1993;48:7003-7010.
34. Fan T. *Mathematical Theory of Elasticity of Quasicrystals and Its Applications*. New York: Science Press Beijing Springer Verlag; 2011.
35. Li X-Y. Fundamental solutions of penny-shaped and half-infinite plane cracks embedded in an infinite space of one-dimensional hexagonal quasi-crystal under thermal loading. *Proc R Soc A*. 2013;469:26. 20130023.
36. Dubois J-M. Clarity through complexity. *Nature Mat*. 2010;9:287-288.
37. Engel M, Umezaki M, Trebin H-R, Odagaki T. Dynamics of particle flips in two-dimensional quasicrystals. *Phys Rev B*. 2010;82:134-206.
38. Abe E, Yan Y, Pennycook SJ. Quasicrystals as cluster aggregates. *Nature Mat*. 2004;3:759-767.
39. Mariano PM, Planas J. Self-actions in quasicrystals. *Physica D - Nonlinear Phenom*. 2013;249:46-57.
40. Li Y, Qin Q-H, Zhao M. Analysis of 3D planar crack problems in one-dimensional hexagonal piezoelectric quasicrystals with thermal effect. Part I: Theoretical formulations. *Int J Solids Struct*. 2020;188-189:269-281.
41. Li Y, Qin Q-H, Zhao M. Analysis of 3D planar crack problems in one-dimensional hexagonal piezoelectric quasicrystals with thermal effect. Part II: numerical approach. *Int J Solids Struct*. 2020;188-189:223-232.
42. Li P, Liu Y, Zhang H, Wang Q. Indentation on a half-infinite one-dimensional hexagonal quasi-crystal space by a rigid flat-ended cylindrical indenter with uniform heat flux or temperature. *Mech Mat*. 2019;131:33-46.
43. Zhou Z, Yang Z, Xu W, Yu X, Xu C, Xu X. Evaluation of electroelastic singularity of finite-size V-notched one-dimensional hexagonal quasicrystalline bimaterials with piezoelectric effect. *Theoret Appl Fract Mech*. 2019;100:139-153.
44. Li W, Shi Y. Extension of elastic models to decagonal quasicrystals. *Crystals*. 2020;10:469.
45. Schmicker D, van Smaalen S. Dynamical behavior of aperiodic intergrowth crystals. *Int J Mod Phys B*. 1996;10:2049-2080.
46. Rochal SB, Lorman VL. Minimal model of the phonon–phason dynamics in icosahedral quasicrystals and its application to the problem of internal friction in the i-AlPbMn alloy. *Phys Rev B*. 2002;144204(1-9):66.
47. Bisconti L, Mariano PM. Existence results in the linear dynamics of quasicrystals with phason diffusion and non-linear gyroscopic effects. *Multiscale Mod Simulation*. 2017;15:745-767.
48. Mariano PM, Salvatori L. Spatial decay of the phason field in quasicrystal linear elasticity. *Mod Sim Mat Sci Eng*. 2015;23:19. 045004.
49. Ricker M, Bachteler J, Trebin H-R. Elastic theory of icosahedral quasicrystals—application to straight dislocations. *Eur Phys J B*. 2001;23:351-363.
50. Amazit Y, Fischer M, Perrin B, Zarembowitch A. Ultrasonic investigations of large single AlPdMn icosahedral quasicrystals. In: Proceedings of the 5th International Conference on Quasicrystals C Janot, R Mossieri (Herausgeber), eds. Singapore: World Scientific; 1995; 584-587.
51. Letoublon A, de Boissieu M, Boudard M, Mancini L, Gastaldi J, Hennion B, Caudron R, BellissentR. Phason elastic constants of the icosahedral Al–Pd–Mn phase derived from diffuse scattering measurements. *Phil Mag Lett*. 2001;81:273-283.
52. Bruggi M, Venini P. A mixed FEM approach to stress-constrained topology optimization. *Int J Num Meth Eng*. 2008;73:1693-1714.

How to cite this article: Bosi A, Mariano PM, Salvatori L. Micro-to-macro interactions in complex bodies: Wavelet-based post-processing detection. *Math Meth Appl Sci*. 2021;1–23. https://doi.org/10.1002/mma.7429